The Astrophysical Journal, 683:1085–1103, 2008 August 20

GAS AND DUST ASSOCIATED WITH THE STRANGE, ISOLATED STAR BP PISCIUM

B. Zuckerman,[1,2] C. Melis,[1] Inseok Song,[3,4] David S. Meier,[5,6] Marshall D. Perrin,[7] Bruce Macintosh,[8] Christian Marois,[8] Alycia J. Weinberger,[9] Joseph H. Rhee,[1] James R. Graham,[7] Joel H. Kastner,[10] Patrick Palmer,[11] T. Forveille,[12] E. E. Becklin,[1,2] D. J. Wilner,[13] T. S. Barman,[14] G. W. Marcy,[7] and M. S. Bessell[15]

Received 2007 August 13; accepted 2008 January 24

ABSTRACT

We have carried out a multiwavelength observational campaign demonstrating some of the remarkable properties of the infrared-bright variable star BP Psc. Surrounded by a compact dusty, gaseous disk, this little-studied late G (or early K) type star emits about 75% of its detected energy flux at infrared wavelengths. Evidence for accretion of gas in conjunction with narrow bipolar jets and Herbig-Haro objects is apparently consistent with classification of BP Psc as a pre–main-sequence star, as postulated in most previous studies. If young, then BP Psc would be one of the nearest and oldest known classical T Tauri stars. However, such an evolutionary classification encounters various problems that are absent or much less severe if BP Psc is instead a luminosity class III post–main-sequence star. In this case, it would be the first known example of a first-ascent giant surrounded by a massive molecular disk with accompanying rapid gas accretion and prominent jets and HH objects. In this model, the genesis of the massive dusty gaseous disk could be a consequence of the envelopment of a low-mass companion star. Properties in the disk may be conducive to the current formation of planets, a gigayear or more after the formation of BP Psc itself.

Subject headings: planetary systems: protoplanetary disks — stars: general

Online material: color figures

1. INTRODUCTION

As laboratories for the early stages of the formation of planetary systems, T Tauri stars have engaged the energy of astronomers for decades. It is desirable to find those closest to Earth because orbiting gas, dust, and protoplanets can be studied with higher linear resolution, that is, smaller semimajor axes. Young stars are usually found in the Galactic plane. As a consequence, specific effort has been expended to find T Tauri stars at high Galactic latitudes because these promise to be relatively close to Earth. In addition, classical T Tauri stars are bright infrared sources and are almost always associated with interstellar molecular nebulosity. Thus, early searches for nearby T Tauri stars focused on bright *IRAS* sources and interstellar molecular clouds at high Galactic latitude (de la Reza et al. 1989; Gregorio-Hetem et al. 1992; Magnani et al. 1995). Two decades of research have demonstrated that neither interstellar molecular clouds nor T Tauri stars substantially younger than 10 Myr are to be found closer to Earth than ~100 pc. And by 10 Myr most T Tauri stars are of the weak-lined, rather than classical, variety. Two well-studied, infrared-bright, nearby classical T Tauri stars are the apparently single TW Hya (Qi et al. 2006 and references therein; 56 pc from Earth) and the close binary V4046 Sgr (Stempels & Gahm 2004; Gunther et al. 2006; ~80 pc from Earth).

BP Psc is a high Galactic latitude ($b = -57^\circ$), bright *IRAS* source that generally has been classified as a T Tauri star. Yet, remarkably, BP Psc (also known as StHα 202) has been almost completely overlooked by the astronomical community. The star has been included in a few surveys, but, to the best of our knowledge, it has never been the focus of any published paper. We present here a suite of optical, infrared, and millimeter wavelength measurements of this extremely interesting, long-neglected star. Notwithstanding that these data, some of which date back a decade, generally support a T Tauri star classification, overall the data appear more consistent with a post–main-sequence evolutionary state. If so, then BP Psc possesses several properties never before observed in a first-ascent giant star. Ultimate resolution of the mystery of the evolutionary state of BP Psc will require a direct measurement of its trigonometric parallax.

2. OBSERVATIONS

2.1. *Millimeter and Centimeter Wavelengths*

CO spectra and continuum emission were investigated with the 15 m JCMT and the 30 m IRAM antennas and the Owens Valley Radio Observatory (OVRO), SMA,[16] and VLA[17] interferometers.

[1] Department of Physics and Astronomy, University of California, Los Angeles, CA 90095.
[2] UCLA Center for Astrobiology, Los Angeles, CA 90095.
[3] Gemini Observatory, Hilo, HI 96720.
[4] Current address: *Spitzer* Science Center, California Institute of Technology, Pasadena, CA 91125.
[5] David S. Meier is a Jansky Fellow of the National Radio Astronomy Observatory.
[6] National Radio Astronomy Observatory, Socorro, NM 87801.
[7] Department of Astronomy, University of California, Berkeley, CA 94720.
[8] Institute of Geophysics and Planetary Physics, Lawrence Livermore National Laboratory, Livermore, CA 94551.
[9] Department of Terrestrial Magnetism, Carnegie Institution of Washington, Washington, DC 20015.
[10] Rochester Institute of Technology, Rochester, NY 14623.
[11] Department of Astronomy and Astrophysics, University of Chicago, Chicago, IL 60637.
[12] Laboratoire d'Astrophysique de Grenoble, Université J. Fourier, 38041 Grenoble, Cedex 9, France.
[13] Harvard-Smithsonian Center for Astrophysics, Cambridge, MA 02138.
[14] Lowell Observatory, Flagstaff, AZ 86001.
[15] Research School of Astronomy and Astrophysics, Institute of Advanced Studies, Australian National University, Canberra, ACT 2611, Australia.

[16] The Submillimeter Array is a joint project between the Smithsonian Astrophysical Observatory and the Academia Sinica Institute of Astronomy and Astrophysics and is funded by the Smithsonian Institution and the Academia Sinica.
[17] The Very Large Array of the National Radio Astronomy Observatory is a facility of the National Science Foundation operated under cooperative agreement by Associated Universities, Inc.

TABLE 1
CO Observations with the JCMT and IRAM 30 m Telescopes

Telescope	Date (UT)	FWHP (arcsec)	Molecule	Transition	Frequency (MHz)
JCMT	1996 Feb	14	CO	$J = 3–2$	345796.0
IRAM (30 m).....	1996 May	11	CO	$J = 2–1$	230538.0
	1996 Jun	11	^{13}CO	$J = 2–1$	220398.7

Single-dish and SMA and OVRO interferometer particulars appear in Tables 1 and 2, respectively. Results from these two millimeter-wavelength interferometers are summarized in Table 3. The CO spectra from four telescopes are displayed in Figure 1. The interferometric CO maps appear in Figure 2.

The JCMT receiver B3i was used for measurement in the 345 GHz atmospheric window. The back end was the Digital Autocorrelation Spectrometer (DAS), with a bandwidth of 250 MHz, which yielded a spectral resolution of 189 kHz. Data were obtained in beam-switching mode. Integration time was 95 minutes at the $J = 3–2$ CO transition. To convert from antenna temperature to main-beam brightness temperature, we applied an aperture efficiency of 0.49. At the IRAM 30 m the "front end" was an SiS receiver and the spectrometer was a 256 channel filter bank with 1 MHz resolution. Data were obtained in beam-switching mode. Integration time was 106 minutes at the 2–1 CO transition and 245 minutes for 2–1 ^{13}CO, but in two polarizations that were then averaged together. To convert from antenna to main-beam brightness temperature, we applied an aperture efficiency of 0.53.

Aperture synthesis observations of the ^{12}CO(2–1) transition of BP Psc were made with the OVRO Millimeter Interferometer between 1996 March 9 and 1997 January 10 (UT). The interferometer consisted of six 10.4 m antennas with cryogenically cooled SiS receivers (Padin et al. 1991; Scoville et al. 1994). Observations in "Equatorial" and "High" configurations were obtained, with system temperatures (single sideband) ranging between 700 and 1400 K at 230 GHz. One hundred twelve 0.538 MHz channels covered the transition with a velocity resolution of 0.70 km s^{-1}. Simultaneous wideband (1.0 GHz) continuum observations were obtained at 3 mm (96.627 GHz) and 1 mm (230.55 GHz). The data set was calibrated using the MMA software package. The phase was calibrated by observing the quasar 3C 454.3 every 18 minutes. Absolute flux calibration was done using Neptune as the primary flux calibrator and 3C 454.3, 0528+134, and 3C 84 as secondary flux calibrators. Absolute flux calibration is estimated to be good to ~10% at 3 mm and ~25% at 1 mm. All subsequent data analysis and manipulation employed the NRAO AIPS package. The OVRO primary beam is ~32″ at 230 GHz. Corrections for the primary beam have not been applied. The longest spatial scales sampled are ~11″ for CO(2–1).

We observed BP Psc with the SMA on 2006 September 26 (UT) using seven antennas that provided baseline lengths from 14 to 69 m. The correlator was configured for the full 2 GHz bandwidth with uniform channel spacing 0.8125 MHz, or 0.7 km s^{-1} at the CO $J = 3–2$ line frequency centered in the USB. Calibration of complex gains was performed by interleaving 4 minute observations of the quasars 3C 454.3 (3.4 Jy) and 2225−049 (1.6 Jy) with 10 minute observations of BP Psc, which was observed over the hour angle range −4 to +4. The system temperatures (DSB) ranged from 175 to 400 K. The absolute flux scale was determined through observations of Uranus, with an estimated uncertainty ≲20%. The naturally weighted CO(3–2) beam size was 2.4″ × 2.0″ at P.A. = 29° (Table 2). The rms noise level for the continuum image (Fig. 3), combining the lower and upper sidebands (effective bandwidth ~4 GHz), was 2.5 mJy. The SMA primary beam is 35″ FWHM at 346 GHz. The data calibration was performed using the MIR software, followed by standard imaging and deconvolution using MIRIAD.

We observed BP Psc with the VLA on 2007 January 28 for a total of 1 hr (including all calibrations). The array was in the DnC configuration. The observations were at X band (on source 20 minutes) and L band (on source 13 minutes) with the default settings for 50 MHz bandwidth. At both frequencies the phase calibration source was 2330+110 and the absolute flux calibrator was 0137+331 (3C 48). Nominally, 27 antennas were in use, but two did not provide any useful data. The operator noted intense radio frequency interference most of the time at L band. The X-band image covers an area of 10.2′ × 10.2′, and the final L-band image covers an area of 51.2′ × 51.2′.

2.2. *Infrared*

Spectra, photometry, and adaptive optics (AO) imaging were obtained in the mid- and near-IR with instruments on the Keck and Gemini telescopes at Mauna Kea Observatory. BP Psc was observed with the Keck Observatory AO system (Wizinowich et al. 2006) and the facility IR camera NIRC2 on 2006 July 19 (UT). At J, H, K', and L' wave bands we obtained four images, each consisting of 50 co-adds with 0.2 s exposure time. We also observed a nearby point-spread function (PSF) reference star of similar brightness. The reference star images have an FWHM of 0.050″ at K' with a Strehl ratio of 0.3; the H images have an FWHM of 0.045″ and a Strehl ratio of 0.18. The PSF reference star is clearly pointlike, indicating that the elongation of BP Psc seen in Figure 4 is not an AO artifact. We used Lucy-Richardson deconvolution to enhance the resolution of the BP Psc images. Figure 4 shows H- and K'-band images of BP Psc together with the PSF reference star and the deconvolved images.

TABLE 2
OVRO and SMA: System Characteristics

Map	Frequency (GHz)	$\Delta V_{\rm chan}$ (km s^{-1})	$\Delta\nu_{\rm band}$ (MHz)	Beam Size (arcsec; deg)	Noise Level (K; Jy beam^{-1})	Detected Flux (%)
CO(2–1)[a].....	230.538	0.70	56	2.35 × 2.23; −75	0.53; 0.12	100
CO(3–2) [NA][b]	345.796	0.71	102.4	2.39 × 1.98; 29	0.37; 0.17	96
CO(3–2) [UN][b]				2.09 × 1.93; 63	0.53; 0.21	90
1.4 mm[a].....	230.55	...	1000	2.30 × 2.18; −77	0.022; 0.0047	...
880 μm[b]	340.886	...	4000	2.46 × 1.96; 27	0.048; 0.0022	...

[a] For observations made from 1996 March 9 to 1997 January 10, with a phase center of $\alpha = 23^{\rm h}22^{\rm m}24.739^{\rm s}$, $\delta = -02^\circ13'41.186''$ (J2000.0); $V_{\rm LSR} = -17$ km s^{-1}.

[b] For observations made on 2006 September 25, with a phase center of $\alpha = 23^{\rm h}22^{\rm m}24.69^{\rm s}$, $\delta = -02^\circ13'41.399''$ (J2000.0); $V_{\rm LSR} = -15$ km s^{-1}.

TABLE 3
OBSERVATIONAL DATA FROM OVRO AND THE SMA

Map	I_{pk}[a] (Jy) (K)	S_{tot}/I_{tot}[b] (Jy km s^{-1}) (K km s^{-1})	V_o[b] (km s^{-1})	$\Delta V_{1/2}$[b] (km s^{-1})	α_o[c] (J2000.0) δ_o (J2000.0)	$\theta_a \times \theta_b$ (arcsec) P.A.[c] (deg)	$^{source}T_{pk}$[d] (K)
CO(2–1)	1.4 ± 0.12	13 ± 0.4	−14.9 ± 0.2[e]	7.0 ± 0.6	23 22 24.64 ± 0.02	1.9 ± 0.2 × 0.73 ± 0.2	24
	6.2 ± 0.5	57 ± 2	−20.9 ± 0.1[e]	2.6 ± 0.3	−02 13 41.52 ± 0.2	91 ± 4	...
1.3 mm	<0.0094	...	...	...	...	...	...
	<0.043	...	...	...	...	...	...
CO(3–2)	3.7 ± 0.17	48 ± 0.2	−17.6 ± 0.13[e]	10.5 ± 0.35	23 22 24.72 ± 0.01	1.8 ± 0.1 × 0.80 ± 0.1	22
	8.0 ± 0.37	100 ± 0.4	...	...	−02 13 41.73 ± 0.1	103 ± 10	...
880 μm	0.018 ± 0.002	...	...	...	23 22 24.72 ± 0.02	0.81 ± 0.2 × <0.2	...
	0.039 ± 0.0044	...	...	...	−02 13 41.55 ± 0.2	∼16	...

[a] Uncertainties are those measured from the map noise. The uncertainties do not include (the larger) absolute flux calibration uncertainties of ∼20%. Upper limits are 2 σ.
[b] Uncertainties reflect the statistical uncertainties of the Gaussian fit only.
[c] For the CO(3–2) data fits are based on the uniformly weighted data set. Uncertainties are estimated as $\theta_{bm} \times [1/(S/N)]$ and do not include any systematic uncertainties.
[d] The implied source brightness temperature based on the fitted source size.
[e] The CO(2–1) line was fitted with two Gaussian components. The two values of each parameter for CO(2–1) represent each fitted component. All velocities are converted to heliocentric assuming $v_{helio} = v_{LSR} - 2.72$ km s^{-1} for BP Psc.

Gemini/MICHELLE mid-infrared photometry and spectra of BP Psc were obtained on 2006 October 4–5 (UT; Table 4 and Figs. 5 and 6). The water vapor (PWV) during the October 4 observations was 5–6 mm, as estimated from converting the 225 GHz optical depth measured at the Caltech Submillimeter Observatory to precipitable water vapor according to Davis et al. (1997). Consequently, there was a high and probably variable infrared background and lower than usual sensitivity. PWV on October 5 was approximately 2.8 mm. A standard chop-nod scheme was employed; only the main beam was used in analysis because the telescope does not guide in the sky beams. Observations of BP Psc were interspersed with those of photometric and telluric spectral standards at similar air mass. Because of the large PWV on October 4, the standard star flux in the MICHELLE filters was estimated by taking the Cohen et al. (1999) template spectrum and multiplying it by both the filter transmission and an ATRAN model of 5 mm PWV. The Si-1 filter is affected by loss of transmission at wavelengths <8 μm through the atmosphere at this high PWV, but the other *N*-band filters are largely unaffected. Quoted flux uncertainties are larger than the statistical uncertainties and were estimated from variability in the standard stars where possible, as well as from experience with mid-IR observations from Mauna Kea.

For the low spectral resolution ($R \sim 200$) *N*-band spectra, wavelength calibration was performed by cross-correlating the telluric ozone feature in both spectra with the high-fidelity spectrum from the National Solar Observatory (Wallace et al. 1994). A small offset (0.2 pixels = 0.004″) in wavelength between the BP Psc and standard spectra produced the lowest noise in the ozone region of the divided spectrum. The measured dispersion was 0.02587 μm pixel^{-1}. The final *N*-band spectrum was normalized to the flux density in the Si-5 filter, which is completely contained within it and in a clear part of the atmospheric window.

Aperture photometry of BP Psc is reported in Table 4. The *N*-band PSF varied in size during the course of the observations. To eliminate any uncertainty associated with aperture corrections, a large, 12 pixel (1.5″ radius) aperture was used for photometry. Uncertainties were estimated from the standard deviation of sky pixels in an annulus at 15–20 pixels. In the case where more than one observation was made at a given wavelength or spectral mode, the results were averaged. The spectra were extracted by summing 9 pixels, approximately twice the FWHM in the spatial direction, centered on the source. Uncertainties at every wavelength were estimated from the standard deviation of sky pixels in a 1″ region 1″ away from the spectrum.

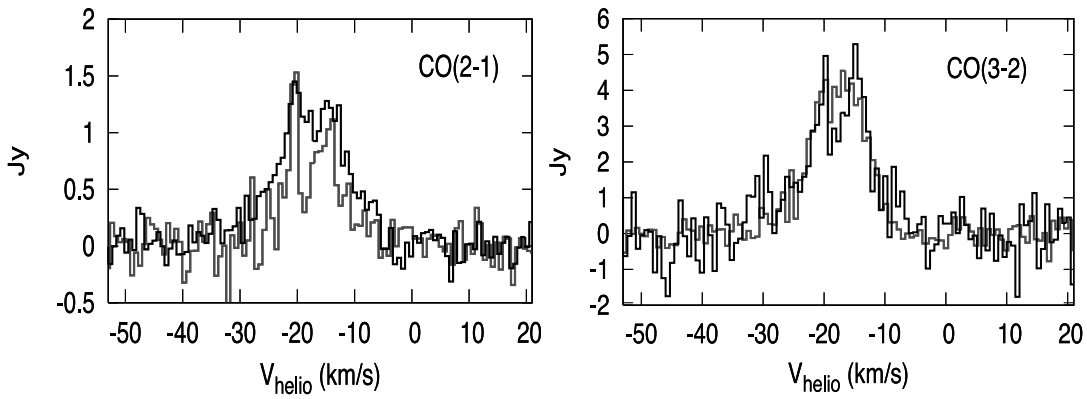

FIG. 1.—Single-dish and interferometer CO spectra of BP Psc. *Left*: Spectra for CO(2–1) from IRAM 30 m (*black line*) and OVRO (*gray line*). *Right*: CO(3–2) with the JCMT (*black*) and SMA (*gray*). All spectra are put on the same flux scale (assuming 3.9 Jy K^{-1} for IRAM and 15.6 Jy K^{-1} for the JCMT) and velocity scale $V_{helio} = V_{LSR} - 2.72$ km s^{-1}. [*See the electronic edition of the Journal for a color version of this figure.*]

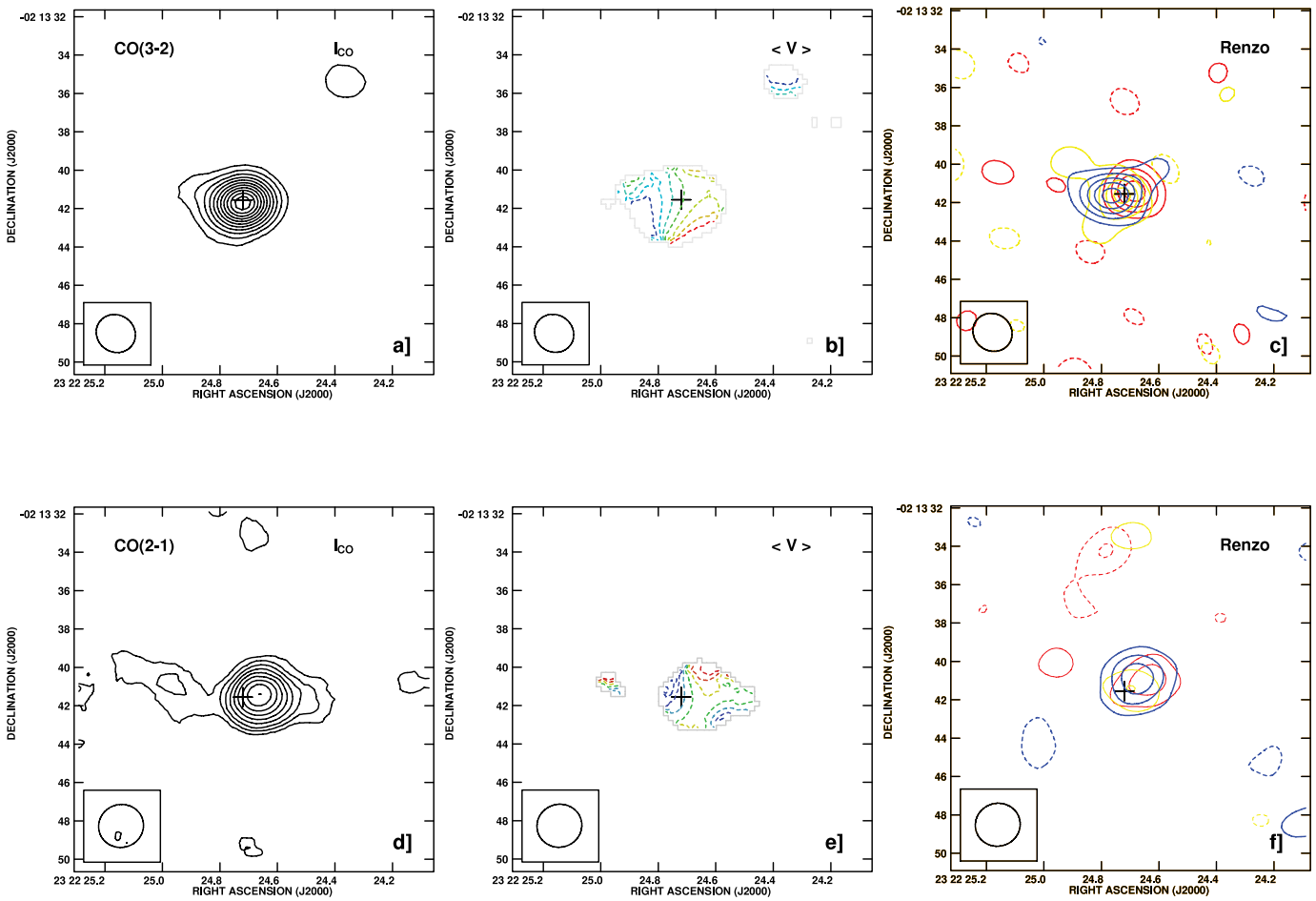

FIG. 2.—(*a*) CO(3–2) uniformly weighted integrated intensity map. Contours are in steps of 2.75 Jy beam^{-1} km s^{-1} (7.0 K km s^{-1}). (*b*) CO(3–2) velocity centroid map. Contours are in steps of 0.4 km s^{-1} ranging from −18.72 (*blue*) to −16.32 km s^{-1} (*red*) (heliocentric). (*c*) CO(3–2) renzogram. Red contours are the −14.7 km s^{-1} channel, yellow the −17.6 km s^{-1} channel, and blue the −20.4 km s^{-1} channel (heliocentric). Contour increments are 3 times the noise levels (σ) listed in Table 2. (*d*) As in (*a*), but for CO(2–1). Contours are in steps of 1.0 Jy beam^{-1} km s^{-1} (4.4 K km s^{-1}). (*e*) As in (*b*), but for CO(2–1). Contours are in steps of 0.33 km s^{-1} starting at −18.66 km s^{-1} (heliocentric). (*f*) As in (*c*), but for CO(2–1). Red contours are the −14.6 km s^{-1} channel, yellow the −17.3 km s^{-1} channel, and blue the −20.1 km s^{-1} channel (heliocentric). Contour intervals are 3 σ. The plus sign in each frame marks the fitted position of the 880 μm continuum source. The beam is displayed at the lower left of each frame.

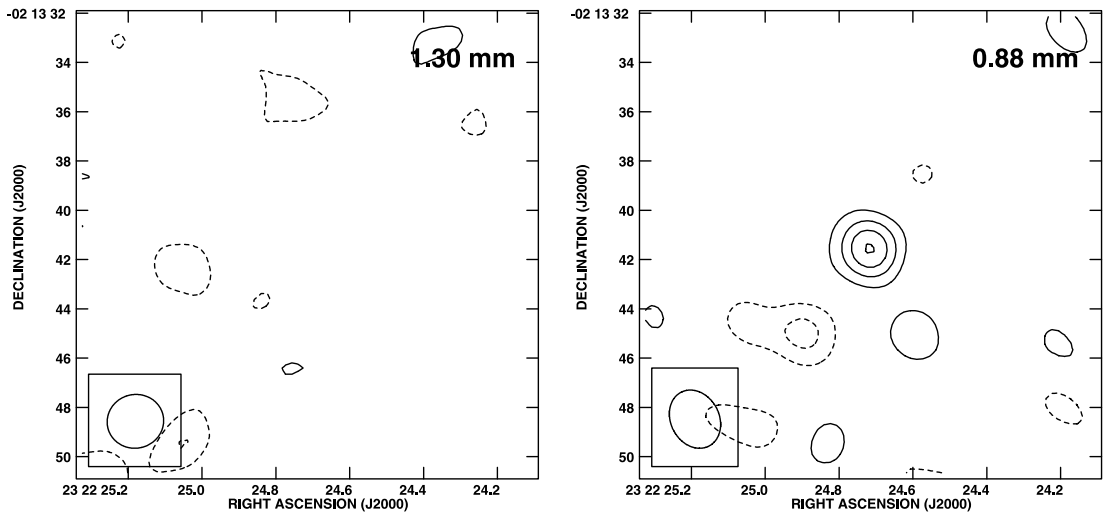

FIG. 3.—Radio continuum images of BP Psc. *Left*: OVRO 230.6 GHz image with contours in steps of 9.4 mJy beam^{-1} or 2 σ. The beam size is plotted in the lower left corner. *Right*: SMA 340.9 GHz continuum image with contours in steps of 4.4 mJy beam^{-1} or 2 σ.

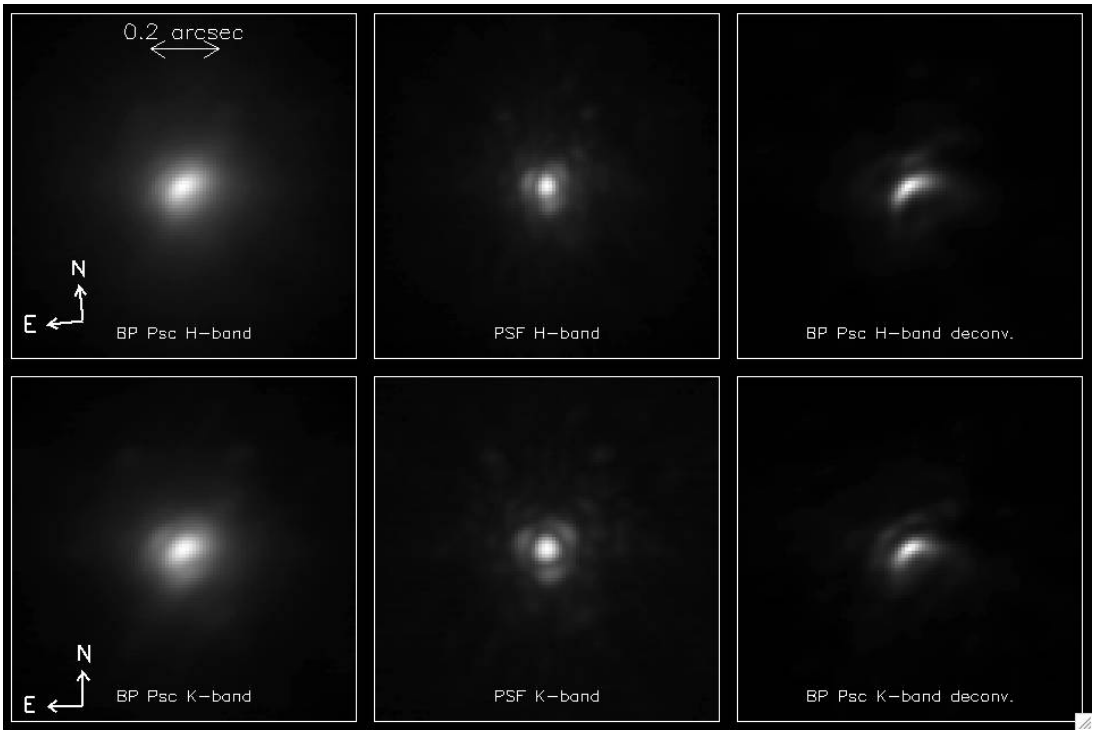

FIG. 4.—*H*- and *K′*-band AO images of BP Psc and a nearby PSF reference star (TYC 5244-226-1). The top row *H*-band images, left to right, are BP Psc, TYC 5244-226-1, and the image of BP Psc deconvolved with a Lucy-Richardson algorithm. Similarly for the bottom row, except at *K′*. All images are 1″ on a side and are presented on a square root intensity stretch. Pixel size is 0.01″.

Near-IR spectra were obtained on 2006 August 9 UT with NIRSPEC (McLean et al. 1998, 2000) on the Keck II telescope (Table 5). In addition, a spectrum in high-resolution mode in the *K*-band window was obtained on 2006 July 22 UT and in low-resolution mode in the *J* band on 2006 August 4 UT.

2.3. *Optical*

We obtained Keck HIRES echelle (Vogt et al. 1994) spectra of BP Psc at five epochs (Table 5 and Figs. 7–9). Wide-field images (Figs. 10 and 11) centered on BP Psc were acquired on 2006 October 23 (UT) with a set of large (4 inch) high-efficiency Hα and [S II] filters recently obtained by J. R. Graham and M. D. Perrin for use with the prime focus camera (PFCAM) on the 3 m Shane telescope at Lick Observatory. Total exposure time with each filter was 40 minutes, but these were mosaicked so not all pixels reached the same sensitivity. In addition, a 420 s exposure was obtained in the continuum with a Spinrad *R*-band filter. The seeing was typical for Lick, and the measured FWHM of the PSF is $1.67'' \pm 0.07''$. Subsequently, an image of the northeast jet was obtained under better seeing conditions (FWHM $\sim 0.65''$ measured from point sources), with the GMOS camera and *g*-band, *i*-band, and Hα filters at the Gemini North Observatory (Fig. 12); exposure times in the three filters were 210, 210, and 1800 s, respectively.

A low-dispersion spectrum was taken on 2007 May 25 18:10 UT with the ANU Double Beam Spectrograph (DBS) on the 2.3 m telescope at Siding Spring Observatory. The resolution in the blue, between 3300 and 5200 Å, was about 3 Å, and about 5 Å in the red between 6300 and 10000 Å. The overall shape of the DBS

TABLE 4
BP PSC MICHELLE MID-INFRARED PHOTOMETRY

Filter	Central Wavelength (μm)	Flux Density (Jy)	Uncertainty (Jy)
Si-1	7.7	1.40	0.10
Si-2	8.8	1.34	0.04
N′	11.2	1.89	0.06
Si-5	11.6	1.84	0.06
Si-6	12.5	2.11	0.06
Qa	18.1	5.2	0.3

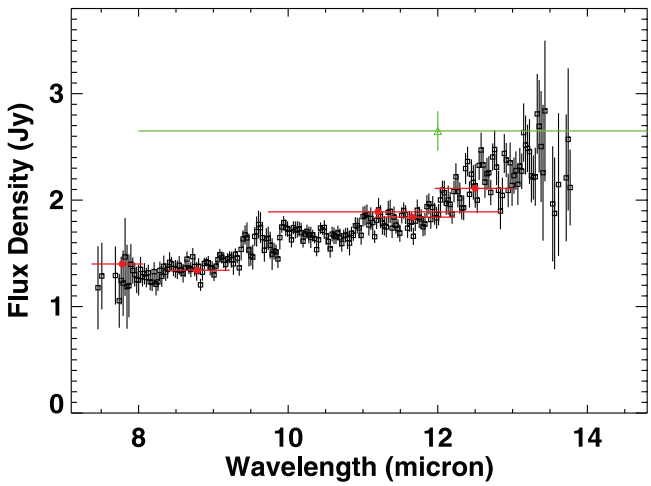

FIG. 5.—Spectrum (*squares*, extending from 7.5 to 13.7 μm) obtained with the MICHELLE spectrometer at the Gemini North Observatory. Also shown are the flux densities and bandpass coverage of five photometric MICHELLE filters (*circles*) and the broad *IRAS* 12 μm filter (*triangle*) with flux density that lies above the flux density of the five MICHELLE filters. As noted in § 3, the little wiggles near 9.5 μm are due to imperfect telluric ozone cancellation and not to a silicate emission feature in BP Psc.

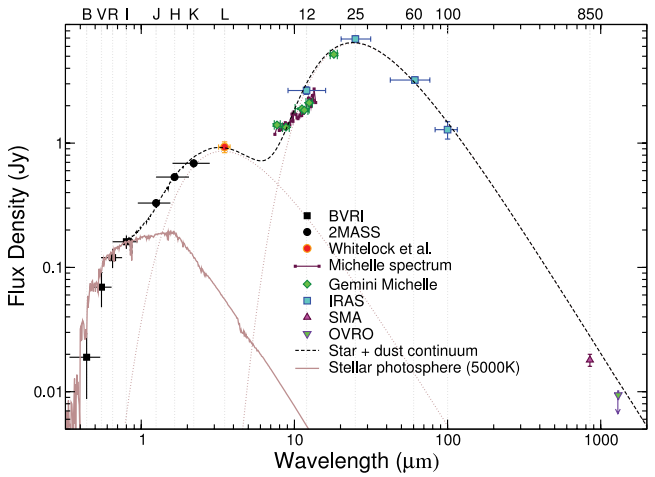

FIG. 6.—SED of BP Psc. As described in § 3, the optical points have been fitted with a 5000 K photosphere. *JHK* data points (*black circles*) are from 2MASS. The L-band point (*orange circle*) is from Whitelock et al. (1995). The green diamonds are from Table 4. The 880 μm and 1.3 mm points are from Table 3. The blue squares are from *IRAS*. The mid-IR spectrum is from Fig. 5. The two dotted lines are 1500 and 210 K blackbodies.

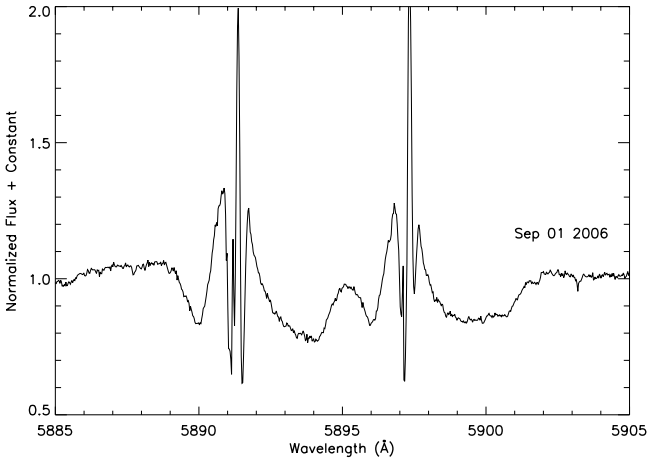

FIG. 7.—Complex sodium D1 and D2 lines, epoch 2006 September 1. For Figs. 7–9, the wavelength scale is corrected to the heliocentric rest frame. One or more of the narrow absorption lines may be interstellar. The wavelength scales in Figs. 7–9 are in vacuum.

spectrum agrees well with one obtained with the 3.6 m ESO telescope at La Silla Observatory (Suarez et al. 2006; O. Suarez 2007, private communication). The DBS blue spectrum (Fig. 13) showed strong emission in the Ca H and K lines, as well as emission at 4068 Å.

3. RESULTS

Perhaps the earliest indication that BP Psc is an unusual star was the 1996 single-antenna radio observations of Table 1 and Figure 1. Very few nearby, high Galactic latitude, isolated, main-sequence and pre–main-sequence stars have detectable CO pure rotational emission; TW Hya and 49 Cet are probably the most noteworthy (e.g., Zuckerman et al. 1995a). No first-ascent giant star is known to display such radio emission. The double-peaked single-dish spectra showed that probably the CO at BP Psc is distributed in an orbiting ring. A nondetection of the ^{13}CO $J = 2$–1 transition with the IRAM 30 m telescope at a level 7 times fainter than the ^{12}CO $J = 2$–1 line implies a ^{12}CO opacity <14 if the isotope ratios are solar (1/89). This result indicates that the CO lines are not very optically thick and that the molecular disk is substantially less massive than disks orbiting some young T Tauri stars located near molecular clouds (see § 4.7).

The single-dish spectra can be compared with the SMA and OVRO spectra to ascertain whether the interferometers are detecting all of the CO emission. Figure 1 shows this indeed to be the case, and the last column of Table 2 indicates that the interferometers detect essentially all the flux seen with the 30 m and JCMT. The SMA spatial resolution was (barely) sufficient to resolve the region of CO(3–2) line emission along a position angle consistent with that of the dust disk implied by our Keck AO images (Fig. 4 and below). The SMA detection of 0.88 mm continuum emission (Table 3 and Fig. 3) enables an estimation of the mass in dust particles orbiting BP Psc (§ 4.6). Given the presence of bipolar jets emanating from BP Psc, radio continuum emission might be detectable (e.g., Reipurth & Bally 2001), but the results of our VLA observations were negative (§ 4.9).

Turning to the infrared and optical, our Keck AO images show a curved morphology with no central point source consistent with a near–edge-on disk optically thick at near-IR wavelengths (Fig. 4). The sky-projected position angle of the major axis of

TABLE 5
JOURNAL OF HIRES AND NIRSPEC OBSERVATIONS

Instrument	UT Date	Spectral Range	Spectral Resolution	Hα EW (Å)	Heliocentric Radial Velocity (km s^{-1})
HIRES	1996 Jul 11	3840–6260[a]	65816	...	−14.74 ± 1.71
	1996 Oct 10	3810–6235[a]	65296	...	−11.46 ± 1.73
	2006 Sep 1	5690–8550[a]	40646	−12.95 ± 0.30	−15.53 ± 0.79
	2006 Sep 9	5690–8670[a]	41263	−15.20 ± 0.36	−14.14 ± 0.83
	2006 Oct 15	3720–7992[a]	51344	−11.37 ± 0.40	−13.20 ± 1.47
NIRSPEC	2006 Aug 9	1.50–1.78[b]	2000	...	...
	2006 Aug 9	2.01–2.44[b]	2000	...	...
	2006 Aug 9	2.83–3.66[b]	2000	...	...
	2006 Aug 9	1.15–1.32[b]	18750	...	...

NOTES.—The 0.79 km s^{-1} radial velocity uncertainty given for 2006 September 1 includes all uncertainties, including those in the velocity of the standards (see § 4.5). The uncertainties listed for 2006 September 9 and October 15 are based on cross-correlation with the 2006 September 1 spectrum and are derived by adding, in quadrature, the 0.79 km s^{-1} September 1 uncertainty and the uncertainty derived from the cross-correlation. Relative to the radial velocity on 2006 September 1, the velocity on September 9 was less negative by 1.39 ± 0.23 km s^{-1}, while the difference between the October 15 and September 1 velocity was 2.33 ± 1.23 km s^{-1}. Derivation of the 1996 epoch velocities and errors is discussed in § 4.5.

[a] In units of Å.

[b] In units of μm.

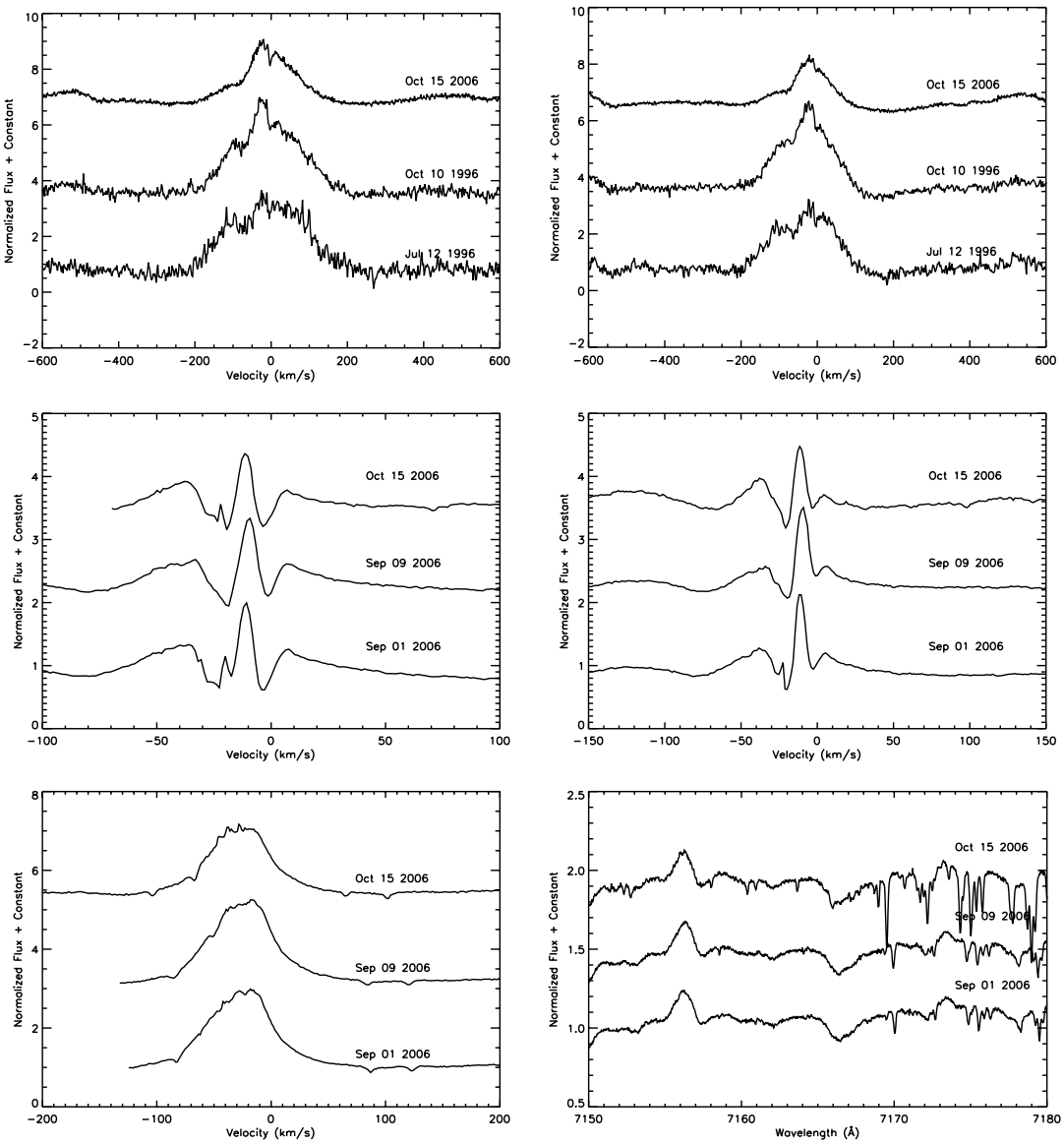

FIG. 8.—Multiple epochs of HIRES spectra. The indicated radial velocities apply to the designated transitions. *Top left*: C II K line. *Top right*: C II H line. *Middle left*: Sodium D2 line. *Middle right*: Sodium D1 line. *Bottom left*: [O I] λ6302 line. The associated [O I] λ6365.5 line is also in emission. *Bottom right*: [Fe II] $\lambda\lambda$7157.1 and 7174.0 doublet emission. Line wavelengths are from "The Atomic Line List 2.05" (http://www.pa.uky.edu/~peter/newpage/). The narrow variable lines are telluric.

the disk lies (somewhere) in the range between 113° and 123°, east of north. Comparison with disk modeling in Burrows et al. (1996) and Wood et al. (1998) suggests a disk inclination of 70°–80° (0° is face-on). The Earth-facing polar axis of the disk lies at a position angle in the range 203°–213°. That is, the side of the disk tilted slightly so that it comes into view along our line of sight is to the southwest. In the deconvolved images, some hint of the side of the disk that is tipped away from us (to the northeast) is visible, the classic morphology of a near–edge-on T Tauri disk (e.g., Burrows et al. 1996). However, the BP Psc disk, of visible extent $<0.2''$, is much more compact than those seen in Taurus. The AO images indicate that only light scattered toward Earth by a portion of the disk is seen in the *JHK* filters, but not the star itself. Consequently, we can be quite sure that the star is not seen directly at any optical wavelength.

Figure 6 displays the spectral energy distribution (SED) of BP Psc. To derive the total energy flux received at Earth, we combine the flux from a 5000 K blackbody with that from two colder blackbodies at 1500 and 210 K to represent the infrared emission from the disk. While this model for the SED is not unique, it produces a reasonable match to the data and implies the presence of very hot dust, consistent with the evidence for *J*- and *H*-band excesses in classical T Tauri stars presented by Cieza et al. (2005) and references therein. The flux decomposition indicates excess emission from BP Psc even in the *J* band. Overall, ~75% of the bolometric luminosity of the star, as seen from Earth, is reprocessed by the orbiting dust grains and reemitted at IR wavelengths. Such a high percentage is unprecedented for a star at high Galactic latitude far from any interstellar molecular cloud (e.g., Fig. 2 in Zuckerman et al. 1995a). In addition, the SED of BP Psc implies the existence of much more warm circumstellar dust than is present around the nearby classical T Tauri stars TW Hya and V 4046 Sgr.

If BP Psc is a pre–main-sequence star, the total luminosity of the system, at each age given in Table 6, can be calculated with the listed radii and a temperature of 5000 K. The corresponding distances (*D*) from Earth listed in the fourth column assume that (1) all of the detected energy under the SED is generated at the

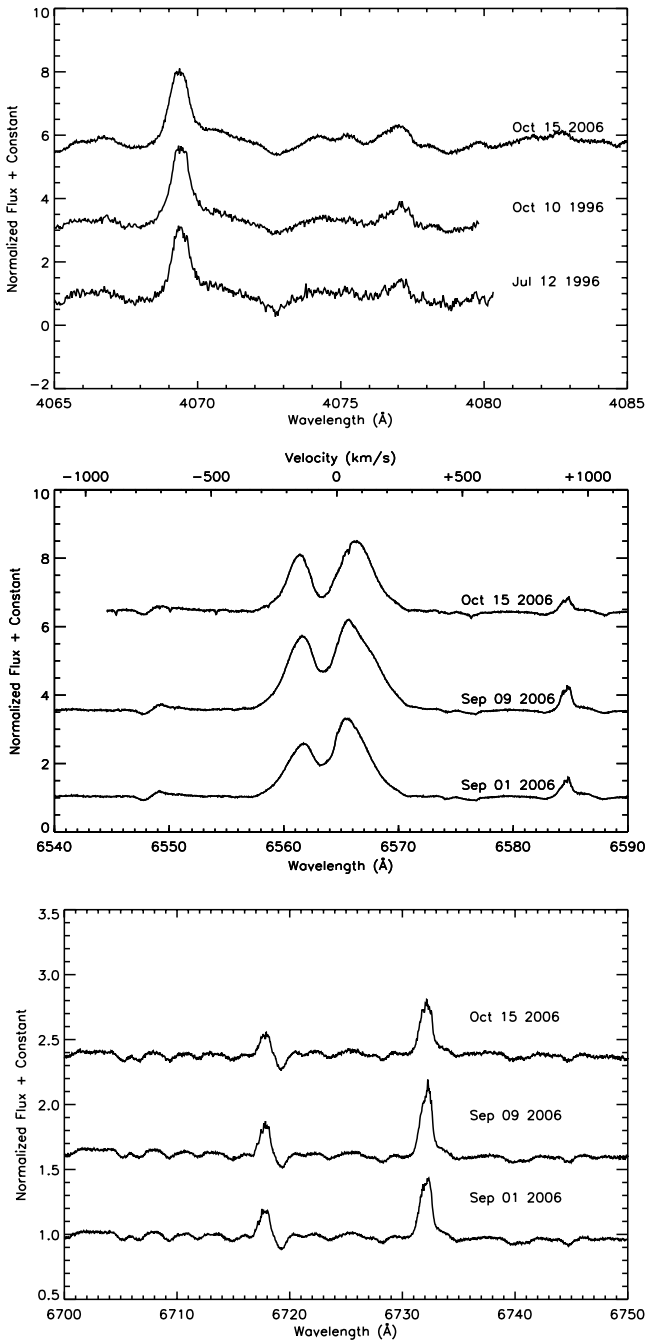

FIG. 9.—*Top*: [S II] $\lambda\lambda$4069.7 and 4077.5 doublet emission. *Middle*: Hα and (much weaker) [N II] $\lambda\lambda$6549.8 and 6585.3 doublet emission. The indicated radial velocities are based on Hα. *Bottom*: Li I λ6709.6 in absorption and [S II] $\lambda\lambda$6718.3 and 6732.7 doublet emission. For lithium, see also Fig. 15.

photosphere of BP Psc and (2) the flux emitted in our direction would not be substantially different if BP Psc were to be observed from a very different direction (e.g., at inclination 0°). However, as some of the observed luminosity can be generated by mass accretion onto BP Psc, and because of the large midplane optical extinction, both assumptions are questionable. When these two effects are estimated and included, revised distances (D') at each young age are listed in the last column of Table 6. Details, as well as consideration of the distance to BP Psc if it is either a pre– or post–main-sequence star, are presented in § 4.3.

The Gemini spectrum (Fig. 5) and photometry are consistent with earlier *IRAS* photometry and, importantly, show little or no indication of any silicate features in the 10 μm window. The wavelength region of 9.3–10 μm includes strong telluric ozone absorption that varies with time and air mass. Although division by the standard star mainly removes its effect, albeit with larger uncertainties at these wavelengths, some residuals appear as wiggles in the spectrum where the slopes of the absorption lines are large.

With NIRSPEC, emission lines are seen from H I Paβ, Brγ, and Pfδ, and also near 1.257 ([Fe II]) and 1.2944 μm (probably due to [Fe II]). Many additional emission lines, both permitted and forbidden, are seen in our HIRES data. The strong, broad Hα emission line is consistent with classification of BP Psc as a classical T Tauri star (§ 4.3). Spectra of young stars with microjets and Herbig-Haro (HH) objects, of the sort seen in Figures 7–9, usually display optical forbidden lines. If a star is surrounded by a dusty disk, viewed close to edge-on, as per BP Psc, then the forbidden lines are usually blueshifted with respect to the systemic velocity. We interpret the central (heliocentric) velocity of the CO $J = 3$–2 line measured with the SMA, -17.6 km s^{-1} (Table 3), to be the velocity of BP Psc. The radial velocities of the [O I], [N II], and [S II] lines displayed in Figures 8 and 9 are blueshifted, typically by about 8 km s^{-1} from this systemic velocity. Although the radial velocity of the photospheric absorption lines is variable (Table 5 and § 4.5), the causes of the variations are still uncertain.

In addition to emission lines from H, Ca, O, N, Fe, and S, emission lines of neutral helium also appear to be present. A weak He I λ5877.2 (vacuum) line appears in all five epoch HIRES spectra with about the same intensity and line shape. By contrast, a more prominent He I emission line appears at 8446.8 Å in both the 2006 September 1 and 9 spectra, but with very different line shapes. A similar striking variation is evident in the shape of the nearby Ca II infrared triplet line at 8500.4 Å.

With moderate-resolution (3.5 Å) spectra, Whitelock et al. (1995) reported the presence in absorption of the G band of CH near 4300 Å and CN bands around 3885 and 4215 Å. Our HIRES spectra show the G band and perhaps the CN bands, while the DBS spectrum (Fig. 13) reveals both the CH and CN bands. The Mg I *b* triplet near 5175 Å is evident in absorption in the HIRES spectra.

Our wide-field optical images (Figs. 10–12) reveal a chain of HH objects extending over a total of $\sim$10′ (Table 7). If BP Psc is a pre–main-sequence star at a distance of 100 pc, then the HH objects are seen over a total linear span >0.3 pc, and over an appropriately greater span if BP Psc is a giant star at a few hundred parsecs. The bipolar outflow extends to the northeast (position angle $\sim$24°) and southwest of BP Psc, consistent with the orientation of the polar axis of the circumstellar disk seen in our Keck AO and SMA images. Based on the disk's apparent inclination (see above), we anticipate that the northeastern jet is redshifted and the southwestern jet blueshifted. Details of the outflow are discussed in § 4.9.

4. DISCUSSION

4.1. *Spectral Type*

As noted in § 3, BP Psc is not directly visible at any optical or near-IR wavelength. Thus, the SED cannot be used to deduce a spectral type. Perhaps this accounts for the varied spectral types that have appeared in the published literature (mid-F, Downes & Keyes 1988; Ae, Gregorio-Hetem et al. 1992; G?, Whitelock et al. 1995). To deduce the spectral type, we compared our HIRES spectra with the spectra of a variety of main-sequence stars without surrounding dust (see Fig. 14). If a dwarf, then the spectral type of BP Psc is early K; we adopt K2 and $T_{\rm eff} = 5000$ K. If BP Psc is

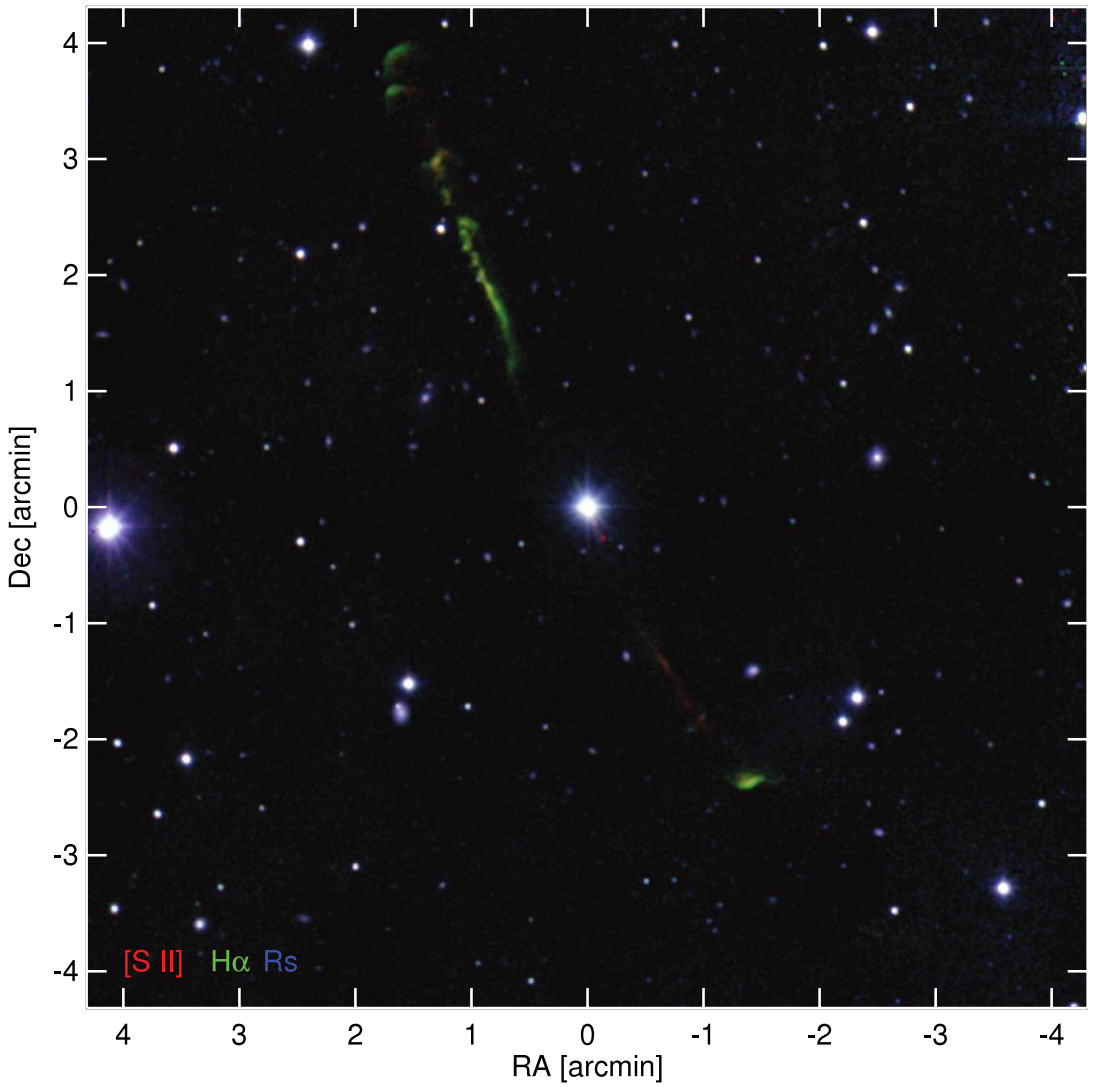

FIG. 10.—Discovery image of outflow from BP Psc showing bipolar narrow emission line jets and HH objects, obtained at Lick Observatory with the 3 m Shane telescope by J. R. Graham and M. D. Perrin. The image, revealing both filamentary structure and bow shocks, is a composite of separate images obtained through narrowband Hα and S II (λ6730) filters and a broadband *R* filter. Blue is *R* continuum, green is Hα, and red is [S II]. The image has been lightly smoothed with a 1.5″ boxcar to highlight faint structure. The nebula is most visible in Hα emission, except for the two knots immediately southwest of the star and a southern filament that appear primarily in [S II]. Note the very faint candidate HH object at (−2.5, −3.5) labeled as knot S6 in Table 7.

a luminosity class III giant star, then, at about this temperature, its spectral type is late G (see § 4.3.2).

While the SED cannot reliably be used to establish the spectral type of BP Psc, the following result from VizieR is noted. VizieR lists measurements of optical broadband colors from a wide variety of sources, obtained at various epochs: nine at *V*-band range over 1.3 mag (11.53–12.85) and five at *R*-band range over 0.5 mag (11.0–11.5). The range in brightness is due to intrinsic variability of this known variable star combined with some measurement error. An average of these brightnesses yields a $V - R$ consistent with an early K-type dwarf or late G-type giant ($V - R \sim 0.7$ mag) with little or no reddening, consistent with the conclusion we draw from our DBS spectrum (§ 4.3.2).

4.2. *Proper Motion*

If the distance to BP Psc were known, then we could decide if it is a giant or a dwarf. But no trigonometric parallax has been measured, and instead we use proper motion to help estimate a distance to BP Psc. The Tycho-2 proper motion of BP Psc is 44.4 ± 4.1 and −26.3 ± 4.3 mas yr^{-1} in right ascension and declination, respectively. Because of its unusual spectrum (e.g., Fig. 7) and variable radial velocities (Table 5 and § 4.5), plausibly, BP Psc might be a close binary star; these often presented problems in measurement of *Hipparcos*/Tycho parallaxes and proper motions. Also, as noted in § 3, Tycho was measuring the position of light scattered off dust orbiting BP Psc, not direct starlight itself. Thus, the Tycho proper-motion measurement could be adversely affected. However, the proper-motion error given above is typical of errors in proper motion of single stars of brightness comparable to BP Psc measured by Tycho. In addition, the Lick Northern Proper Motion Program: NPM1 Catalog (Klemola et al. 1987) gives a proper motion of 36.6 ± 5, −42.6 ± 5 mas yr^{-1}, in reasonable agreement with Tycho, in particular, in the important absolute value of the total proper motion.

We can also use the epoch 2006.7 SMA measurements of the dust emission centroid (Fig. 2) and the epoch 1991.7 Tycho-2 position to check the cataloged Tycho-2 proper motion. The epoch 1991.75, equinox J2000.0, Tycho-2 position is $23^{h}22^{m}24.6666^{s}$, $-02^{\circ}13'41.049''$. The total 15 yr proper motion, based on the Tycho-2 proper motion (see above), is 666 mas in right ascension

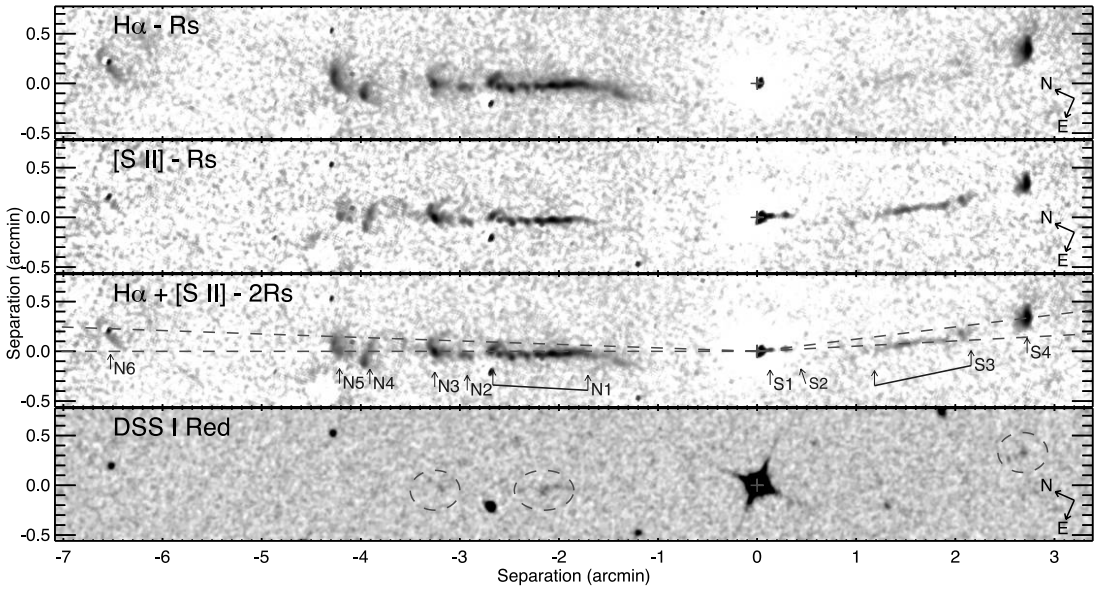

FIG. 11.—*Top panel*: Continuum-subtracted Hα image of the outflow from BP Psc. The plus sign marks the position of BP Psc itself. Due to PSF variations between the Hα and the *R* images, a few subtraction residuals are visible at the positions of the stars in the field. *Second panel*: Continuum-subtracted [S II] image. Note the two knots immediately southwest (right) of BP Psc and the much brighter southwest filament compared to Hα. *Third panel*: Summed Hα and [S II] image, with individual HH clumps labeled. The dashed lines connect BP Psc with some of the brighter clumps. *Bottom panel*: For comparison a digitized Palomar Sky Survey red image. Three of the brightest HH objects are visible (*circled*) in this $\sim$18 yr old plate. Knot S4 appears to have moved about 5$''$ between the DSS epoch and fall 2006, suggesting a proper motion $\sim$0.25$''$ yr^{-1} (see § 4.9). [*See the electronic edition of the Journal for a color version of this figure*.]

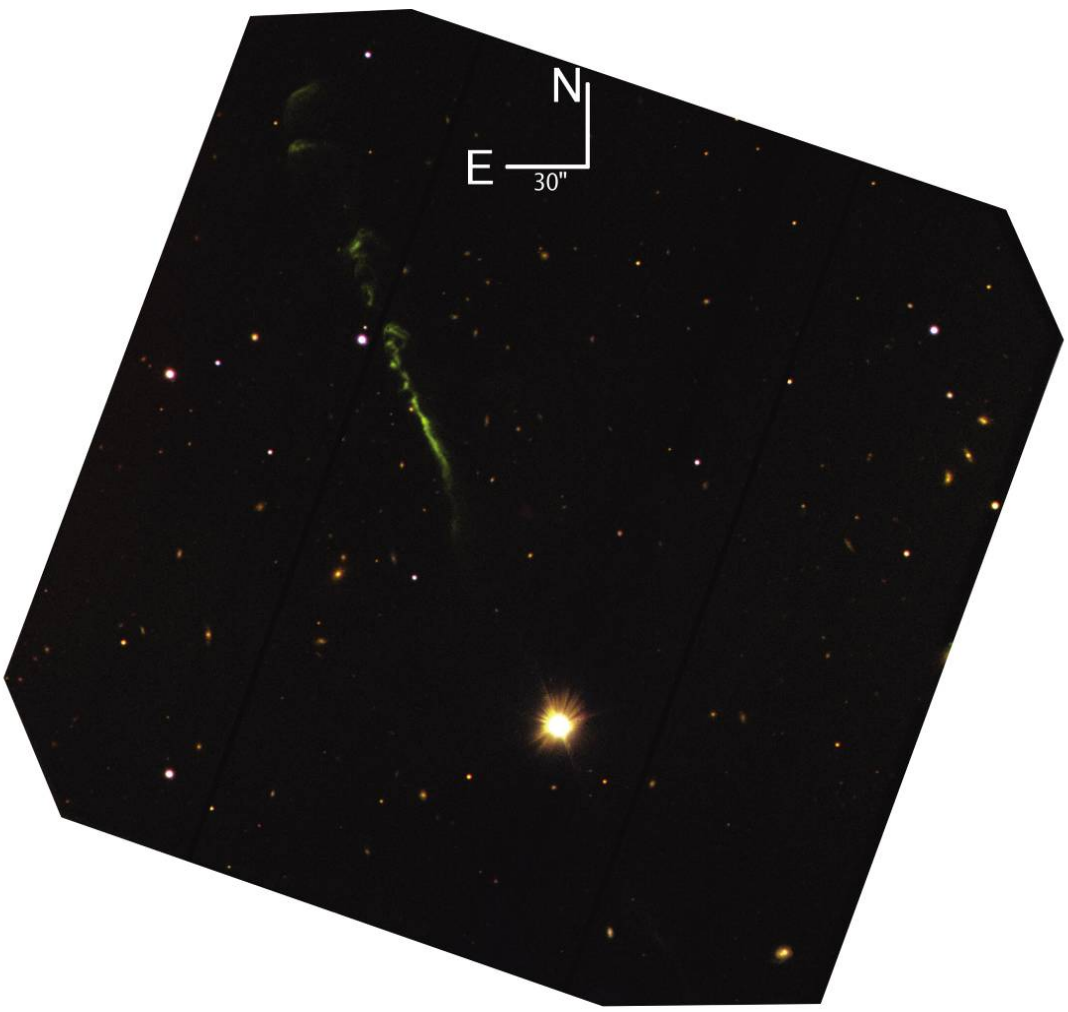

FIG. 12.—Composite image of the northeastern jet obtained with the GMOS camera at the Gemini North Observatory. The images were obtained at air mass of about 2.

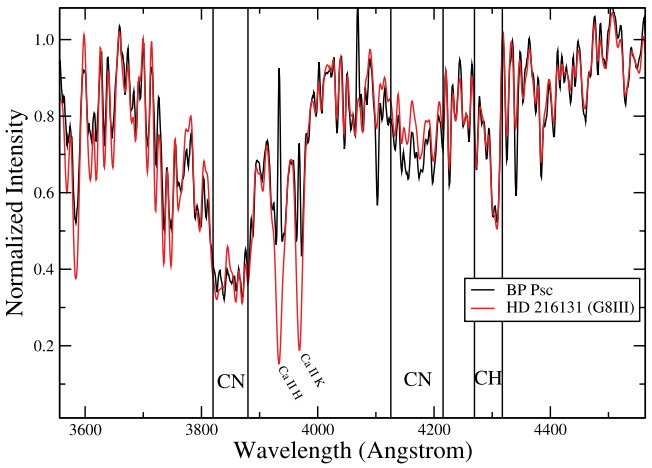

FIG. 13.—BP Psc spectrum obtained with the Double Beam Spectrograph at the 2.3 m telescope at Siding Spring Observatory compared with a rotationally broadened spectrum of a late G-type giant from the MILES database (Sanchez-Blazquez et al. 2006). The CH G band near 4300 Å is evident as are CN bands near 3885 and 4215 Å.

and −394 mas in declination, indicating a J2000.0, 2006.7 epoch position of $23^h22^m24.711^s$, $-02°13'41.44''$. The errors in this position are 150 and 188 mas, respectively, in right ascension and declination, where the errors are derived by adding, in quadrature, the Tycho-2 errors in the 1991.7 position and the proper motion. Within the errors, this Tycho-2 predicted 2006.7 position for BP Psc is in agreement with the SMA measured position (see caption to Fig. 2 and the 880 μm entry in Table 3). In sum, there is no reason to doubt the accuracy of the Tycho-2 proper motion.

4.3. *Distance, Bolometric Luminosity, and Evolutionary State*

In the literature, BP Psc has usually been classified as a T Tauri star. However, such an interpretation is not without its problems as described below. So, in the absence of a direct trigonometric measurement of the distance from Earth of BP Psc, it is prudent to consider alternative evolutionary states.

Some post–asymptotic giant branch (AGB) stars are accompanied by substantial quantities of dust and molecular gas, with a substantial fraction residing in orbiting circumstellar disks (e.g., de Ruyter et al. 2006). Post-AGB stars have bolometric luminosities a few thousand times solar or more. Integrating under the SED (Fig. 6), if BP Psc has a luminosity of 3000 $L_\odot$, then it is 5400 pc from Earth. At a distance of 5400 pc, the Tycho-2 proper motion implies a velocity in the plane of the sky of 1400 km s^{-1}. Clearly, BP Psc is not a post-AGB star.

TABLE 6

BP Psc: PRE–MAIN-SEQUENCE EVOLUTIONARY AND KINEMATIC PROPERTIES

Age (Myr)	M ($M_\odot$)	R ($R_\odot$)	D (pc)	U (km s^{-1})	V (km s^{-1})	W (km s^{-1})	D' (pc)
3	1.72	2.13	157	−21	−36	−4	121
5	1.62	1.88	139	−19	−33	−2	107
10	1.26	1.41	104	−14	−26	+2	80
20	1.04	1.10	81	−12	−23	+5	62

NOTES.—M and R are based on evolutionary models of Baraffe et al. (2003) and I. Baraffe (2006, private communication). Galactic UVW velocities are with respect to the Sun, and U is defined to be positive toward the Galactic center. At all ages the stellar temperature is assumed to be 5000 K. D is the appropriate distance to BP Psc if the integrated flux in Fig. 6 is radiated isotropically and none of this flux is due to accretion of disk material onto BP Psc. D' is the estimated distance to BP Psc when mass accretion luminosity and anisotropic emission are taken into account. See § 4.3.1 for details.

TABLE 7

HERBIG-HARO OBJECTS

Name	R.A.	Decl.	Separation (arcsec)	P.A. (deg)	Comment
N7	23 22 38.7	−02 03 46	631.3	19.4	Very faint
N6	23 22 34.5	−02 07 38	392.0	22.0	Bow shock
N5	23 22 31.3	−02 09 49	252.6	23.1	Bow shock
N4	23 22 31.5	−02 10 06	238.3	25.3	Bow shock
N3	23 22 29.9	−02 10 43	194.7	23.6	
N2	23 22 29.5	−02 11 01	175.9	24.2	
N1	23 22 28.9	−02 11 14	160.3	23.2	Filament end
	23 22 27.6	−02 12 08	103.1	25.0	Filament start
S1	23 22 24.4	−02 13 48	7.9	−146.4	
S2	23 22 24.1	−02 13 57	17.9	−150.5	
S3	23 22 22.7	−02 14 46	71.1	−155.2	Filament start
	23 22 20.4	−02 15 35	130.5	−150.5	Filament end
S4	23 22 19.1	−02 16 03	164.5	−149.4	Bow shock
S5	23 22 14.9	−02 17 21	264.1	−146.3	Very faint
S6	23 22 10.9	−02 18 35	359.1	−144.9	Very faint

NOTES.—HH objects observed around BP Psc, ordered from north to south. Units of right ascension are hours, minutes, and seconds, and units of declination are degrees, arcminutes, and arcseconds. For the long narrow filaments, the coordinates of each end are given. The curvature of the jet is apparent in how the position angles deflect with increasing distance from BP Psc. The outermost knots in both the north and south directions are detected at low S/N in our images and would benefit from additional observations.

4.3.1. *Classical T Tauri Star?*

If BP Psc is a pre–main-sequence star, then its distance from Earth and Galactic space motion (UVW) depend on its age. Table 6 lists some age-dependent properties based on evolutionary models of Baraffe et al. (2003) and I. Baraffe (2006, private communication). Table 6 UVW velocities are similar to the motion of stars in the solar vicinity with ages between about 10 and 100 Myr (Table 7 in Zuckerman & Song 2004; I. Song et al. 2008, in preparation). While not a proof of youth, the fact that, as a dwarf, BP Psc turns out to have the space motion of a young star, rather than some completely different motion, gives weight to a young star interpretation. In addition, the rapid rotation of BP Psc determined from the HIRES spectra ($v \sin i = 32.3 \pm 1.2$ km s^{-1}) is consistent with a very young age. However, as noted in § 3, essentially all the light measured by HIRES has been scattered off the surrounding dust and, hence, Doppler broadened. Thus, the measured $v \sin i$ should be regarded only as an upper limit to the true $v \sin i$ of the star.

The age-dependent distances to BP Psc (fourth column of Table 6) were derived in the following way. First, we fixed the temperature at 5000 K from the HIRES echelle spectrum (§ 4.1). Then we chose an age and found the appropriate stellar radius from the Baraffe et al. models. With this radius and temperature we fitted the optical portion of the SED (Fig. 6) with a 5000 K photospheric model and derived a "5000 K distance" to BP Psc under the assumption that this photospheric emission encompassed all the flux. Obviously, this assumption is wrong because the 5000 K model accounts for only about 25% of the total flux under the SED. We thus corrected the derived 5000 K distances by bringing BP Psc a factor of 2 closer to Earth, and it is these corrected distances, D, that appear in the fourth column of Table 6.

However, two additional phenomena must also be considered. First, as noted in § 4.8, perhaps 20% of the bolometric luminosity of the system is due to accretion of disk material onto BP Psc.

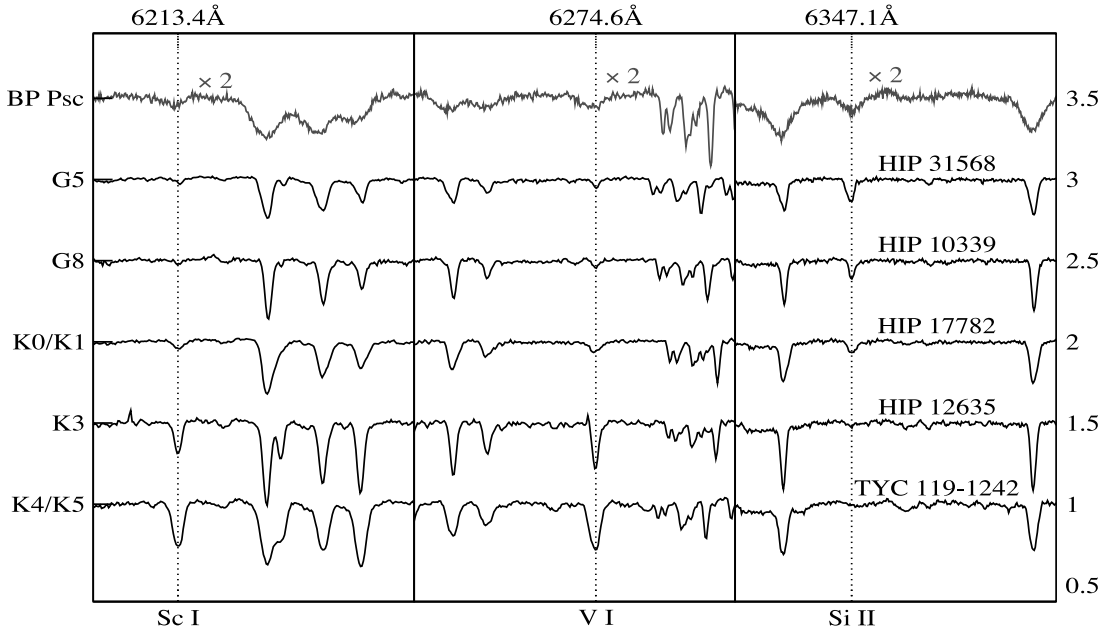

FIG. 14.—Comparison of BP Psc HIRES spectrum with HIRES spectra of five dwarf stars not known to have any surrounding dust (from I. Song et al. 2008, in preparation). From comparison of the line ratios, we deduce that the spectral type of BP Psc, if it is a dwarf, is early K. [*See the electronic edition of the Journal for a color version of this figure.*]

If so, then the distances listed in Table 6 for each Baraffe model would need to be increased by 10%. Given various model uncertainties, this small distance correction, by itself, is "lost in the noise."

A potentially more significant correction to Table 6 distances arises from the location of our viewing angle nearly in the plane of BP Psc's dusty disk. The energy contained under the 210 K blackbody curve in Figure 6 is roughly half the energy under the sum of the 5000 and 1500 K curves. The former is thermal emission from the grains and should be essentially constant independent of viewing angle (because optical depths at these long wavelengths are small). But the shorter wavelength optical plus near-IR light can vary substantially with viewing orientation. Estimates for face-on disks can be obtained from Weinberger et al. (2002) or Low et al. (2005), showing the SED of TW Hya, and from Figure 1*b* in Wood et al. (1998). From these SEDs, we estimate that, for face-on orientations, the short-wavelength flux from BP Psc could be about 7 times the long-wavelength thermal emission (rather than only twice as large, as per Fig. 6). If observed from the same Earth–BP Psc separation but in the face-on disk direction, the total flux received from BP Psc would be about 3 times larger than the flux indicated in Figure 6. Then, if averaged over all 4π sr, the total energy emitted by BP Psc might be about twice what one would deduce from assuming that received flux is independent of viewing orientation and equal to that in Figure 6. If so, then the distances D listed in Table 6 all should be reduced by a factor of 1.4.

The above two correction factors operate in opposite directions, and each is obviously uncertain. Nonetheless, the distances D to BP Psc listed in Table 6 may all be overestimated by a factor of about 1.3. For example, if the Baraffe et al. models are accurate, then if 10 Myr old, BP Psc would be only 80 pc from Earth. Actually, for the Tycho-2 proper motion of 52 mas yr^{-1}, 80 pc would be a more typical young-star distance than 104 pc. In view of the above discussion, in the last column of Table 6, for each age we list distances D' that are a factor of 1.3 times smaller than the distances D listed in the fourth column.

Given the existence of massive amounts of dust (§ 4.6), an orbiting gaseous disk (§ 4.7), and prominent polar jets and HH objects (§ 4.9), if BP Psc is a pre–main-sequence star, then we tentatively adopt an age of $\sim$10 Myr; a still younger age would compound both the weak lithium line problem and the mystery of BP Psc's origin (§ 4.10). The measured equivalent width (EW) of the lithium λ6709.6 line is only 50 mÅ (Figs. 9 and 15), which is more appropriate for a K star of age 100 Myr or greater (Fig. 3 in Zuckerman & Song 2004). We know of no other example of an early K-type star of age 10 Myr with such a weak lithium line. Because significant mass is accreting onto BP Psc (§ 4.8), one should consider the possibility of severe veiling at the Li line, even though veiling at 6700 Å in an early K-type star is usually modest compared to veiling at other wavelengths in typical T Tauri stars (see, e.g., Fig. 5 in White & Hillenbrand 2004). Following the method of Palla et al. (2005), we compared the strength of the $\lambda\lambda$6678 and 6710 lines of Fe I and the λ6768 line of Ni I in BP Psc and in seven main-sequence dwarfs with $V - K$ colors of early K-type stars, but without veiling. In this way we estimate a veiling of about 15% and, at the most, veiling reduces the Li line EW at BP Psc by about 20 mÅ. But even at 70 mÅ, the Li line EW in BP Psc would be characteristic of early K-type stars 100 Myr old or older.

Considering the characteristic long time, hundreds of millions of years, for substantial lithium depletion in early K-type stars, such a weak line is not easily understood if BP Psc is only $\sim$10 Myr old. Other heavily dust-enshrouded, isolated, K-type classical T Tauri stars (e.g., TW Hya, Webb et al. 1999; V4046 Sgr, Stempels & Gahm 2004) have lithium absorption lines with EW $\sim$ 500 mÅ. Indeed, V4046 Sgr is a close binary and both K-type components show these very strong lithium lines.

If BP Psc is 10 Myr old, then it may be the oldest known pre–main-sequence or main-sequence star associated with bipolar jets and HH objects (e.g., Reipurth & Bally 2001). At the corresponding distance of 100 pc or less (Table 6), BP Psc would be the closest known T Tauri star with spatially resolved polar jets (plus HH chains). If it is a pre–main-sequence star, then whatever its precise age, BP Psc clearly should be classified as

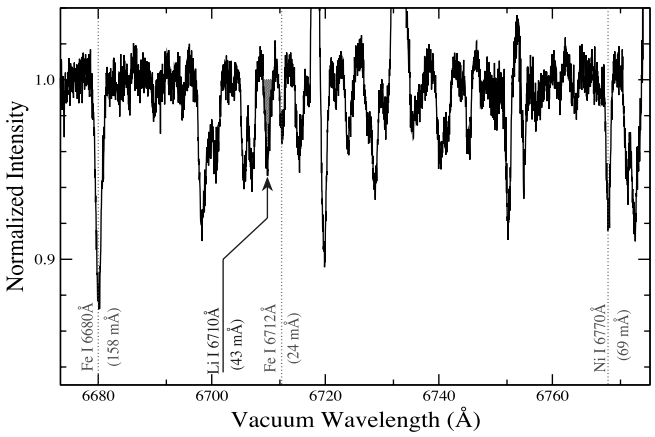

FIG. 15.—Vicinity of the lithium λ6709.6 line in the 2006 September 9 HIRES spectrum. As a consequence of veiling, the measured equivalent width (EW) of the lithium line should be corrected upward as described in § 4.3. Lithium EWs measured on 2006 September 1 and October 15 are consistent with the EW from September 9. [*See the electronic edition of the Journal for a color version of this figure.*]

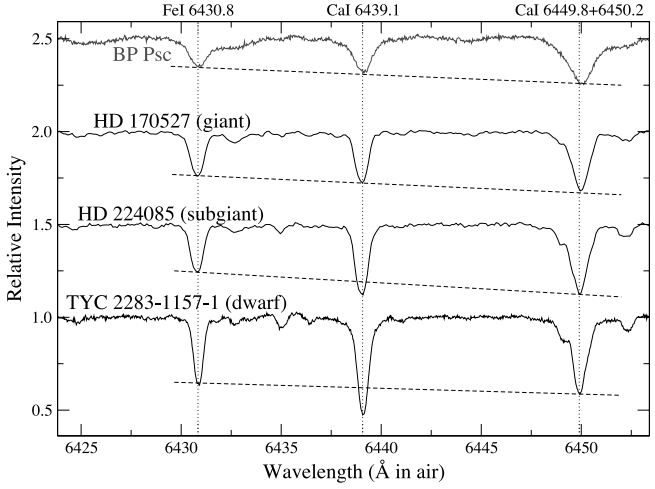

FIG. 16.—Comparison of BP Psc HIRES spectrum with a HIRES spectrum of an early K-type dwarf and KPNO echelle spectra (courtesy of F. Fekel) of a G/K-type giant and subgiant. [*See the electronic edition of the Journal for a color version of this figure.*]

a classical T Tauri star based on the definition of White & Basri (2003; see also Briceno et al. 2007): a star with spectral type in the range K0–K5 with Hα emission equivalent width >3 Å and full width at 10% of peak flux >270 km s^{-1}. Our three measurements of EW (Table 5) are all much larger than 3 Å (see also Gregorio-Hetem et al. 1992), and the 10% width of the Hα line (Fig. 9) is $\sim$500 km s^{-1}.

4.3.2. *First-Ascent Giant or Subgiant Star?*

If BP Psc is a first-ascent giant star, then it is the first one known with a gaseous disk detected in pure rotational CO transitions and undergoing rapid accretion onto the central star. It would also be the first known with bipolar outflow and associated HH objects.

Notwithstanding these unprecedented properties, the data for BP Psc better support first-ascent giant status than any alternative evolutionary state. The lithium line EW is nothing special for a first-ascent giant star; depending on distance, a good match can be made between the kinematic mass and evolutionary mass (see § 4.4); and the Galactic space motions are entirely reasonable for a (few) Gyr old star. For example, at a distance of 300 pc (see § 4.4), $UVW = -38.8, -61.0$, and -21.9 km s^{-1}. The important V component is typical of white dwarfs (e.g., Table 6 in Zuckerman et al. 2003) having ages that are likely to be comparable to that of BP Psc if it has evolved from an A- or F-type main-sequence progenitor. Perhaps the most telling reason why BP Psc is probably a first-ascent giant star are the relative intensities of gravity-sensitive lines, as outlined in the following discussion.

Fekel et al. (1996) used luminosity-sensitive line ratios in the vicinity of 6440 Å to help them deduce that HD 233517 is a dusty, lithium-rich, first-ascent giant star (rather than pre–main sequence). To investigate the luminosity class of BP Psc, we first used iron and calcium lines in our HIRES spectra in this spectral region (Fig. 16). This comparison suggested that BP Psc is probably a giant star or perhaps a subgiant, but probably not a dwarf. Given this result and to better pursue this path, we obtained the DBS spectrum mentioned in § 2.3 and compared it to a variety of spectral standards.

Except for much stronger absorption in Hδ and Hγ, the underlying DBS absorption-line spectrum resembles that of G8 III stars in the MILES database (Sanchez-Blazquez et al. 2006[18]). The blue spectrum of BP Psc does not resemble late G or early K dwarfs because it shows weaker neutral lines of Fe and Mg and strong bands of CN at 4115 and 3889 Å. In Figure 13 the relative F_λ spectrum of BP Psc is shown in comparison with one of these G8 III stars, HD 216131 from the Miles database smoothed to match BP Psc. As well as the line spectrum being a good match, the relative fluxes are in good agreement, indicating that BP Psc has little reddening.

The ELODIE Archive (Moultaka et al. 2004[19]) of echelle spectra also has many late G giants and dwarfs for comparison with the HIRES echelle spectrum of BP Psc. We initially selected a region near 5350 Å that contained several well-defined Fe II and Ti II lines in addition to other lines of neutral species (Fig. 17). The Elodie spectra were again broadened to match the rotationally broadened lines of BP Psc. The comparison indicated clearly that the spectrum of BP Psc resembled that of a luminosity class III star and not a class V or II star. Furthermore, the strongest features in BP Psc were systematically shallower than the same features in the comparison stars, a systematic effect that was eliminated by adopting a 15% veiling of the BP Psc spectrum. Comparison of BP Psc with the same three standard stars, but near 6060 Å, suggests similar conclusions (Fig. 18).

The regions of the Hδ and Hγ lines were also compared in the echelle spectra in order to assess their unusual strengthening in BP Psc. A value of 15% veiling in the blue was also indicated, and anything larger would put the core of Hδ below zero. The hydrogen lines in BP Psc had almost twice the equivalent width of the comparison G8 III stars, and stronger even than in a much hotter F8 III star. In addition, the shape of these two hydrogen lines was quite different from either a G8 III or F8 III star having deeper and wider cores and shallow wings.

Independently, K. Biazzo and A. Frasca at Catania Observatory used their ROTFIT code (Frasca et al. 2003, 2006; Biazzo et al. 2007) to compare several different red wavelength regions in the BP Psc Keck spectrum with stars in the Elodie Archive. They derive a $v \sin i$ of about 38 km s^{-1} for BP Psc, deduce that the spectral type best reproducing these regions was G8–K0 III/IV, and rule out class V dwarfs. Furthermore, a veiling of 15% improved the residual fits and strengthened the giant luminosity identification. They suggest a $T_{\rm eff} \sim 4900 \pm 100$ K and $\log g \sim 2.5 \pm 0.3$.

[18] See also http://www.ucm.es/info/Astrof/miles/miles.html.

[19] See also http://atlas.obs-hp.fr/elodie/.

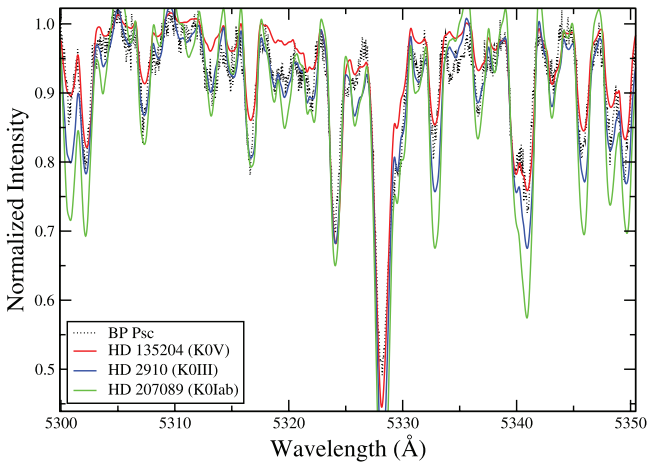

FIG. 17.—Comparison of a BP Psc HIRES spectrum with spectra of a dwarf, giant, and supergiant from the ELODIE Archive (Moultaka et al. 2004) appropriately broadened to match the broad lines of BP Psc. The wavelength scales in Figs. 17 and 18 are in air.

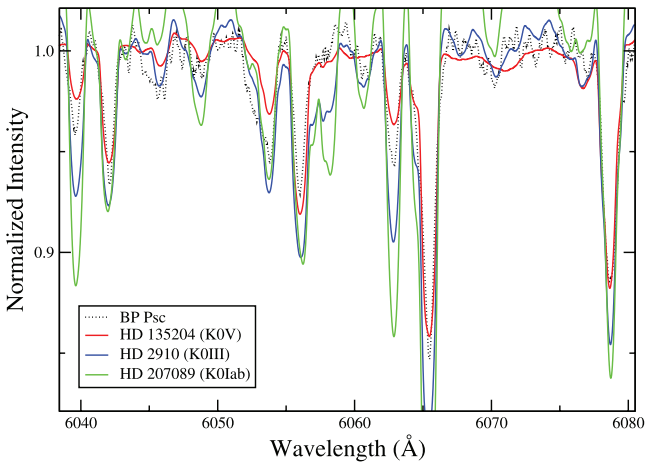

FIG. 18.—Same as Fig. 17, but for a different spectral region.

Although the best fit of surface gravity–sensitive lines demonstrates that BP Psc is a giant instead of a main-sequence star, because young pre–main-sequence stars also have lower surface gravities than do main-sequence stars, one has to check whether a really young star model spectrum of BP Psc can reproduce the above-quoted $\log g$ value (≤ 2.8).

Based on theoretical evolutionary models of Baraffe et al. (1998) and Siess et al. (2000), very young ($\sim$1 Myr) pre–main-sequence stars with effective temperature similar to that of BP Psc ($\sim$5000 K) have $\log g \sim 3.6$–3.7, which is significantly higher than the best-fit value. This strongly supports classification of BP Psc as a post–main-sequence giant of luminosity class III instead of as a young, pre–main-sequence star.

4.4. *Kinematic Mass versus Evolutionary Mass*

Assuming Keplerian revolution, the spatial separation of the blue and red peaks in the SMA CO(3–2) emission map (Fig. 2) can be used to estimate the mass of BP Psc (e.g., Beckwith & Sargent 1993). Neglecting the disk mass (§§ 4.6 and 4.7) compared to the stellar mass (M_*), one can write

$$M_* = R(V_d)^2/G = R\left(V_p\right)^2/G(\sin i)^2, \qquad (1)$$

where R is the CO disk radius, V_d is the Keplerian velocity at R, V_p is the projected velocity along the line of sight, and i is the inclination angle of the disk to the line of sight ($i = 0$ is face-on). From the AO images, we estimate the inclination angle to be $75^\circ \pm 10^\circ$. The separation of the red and blue peaks is $1.2'' \pm 0.20''$ (statistical uncertainty only).

A difficult issue is the value to assign to V_p. According to the Beckwith & Sargent (1993) models, a disk with a sharp outer edge and inclination angle of 75° should display two CO emission peaks with a deep central depression (their Fig. 5). As may be seen in Figure 1, the observed spectral central dip is usually weak or not even present (SMA, 3–2 line). Examination of the interferometer maps and model fits to the line profiles together suggest that V_p lies somewhere in the range 3–4.5 km s^{-1}, with the lower values preferred. For a 10 Myr old star, $V_p = 3$ km s^{-1}, and the Table 6 dust-corrected distance (D') of 80 pc, the derived (kinematic) value of M_* is 0.52 $M_\odot$. If, rather, $V_p = 4$ km s^{-1}, then $M_* = 0.92\ M_\odot$.

The evolutionary model mass of a 5000 K, 10 Myr old star is 1.26 $M_\odot$ (Table 6; Baraffe et al. 2003; I. Baraffe 2006, private communication). For the Baraffe models the ratio of kinematic to evolutionary mass hardly varies for ages between 3 and 20 Myr:

$$M_{\rm kin}/M_{\rm evol} \propto R/D^x \propto D/D^x, \qquad (2)$$

where, from the second and fourth columns of Table 6, the distance dependence of the evolutionary mass goes like D^x, and x is of order unity or slightly less. Hence, the Baraffe model mass appears to be larger than the most likely kinematic mass of a pre–main-sequence star. The discrepancy would be greater yet should BP Psc be a single-lined spectroscopic binary with a faint companion (§ 4.5). However, as the kinematic mass is derived from an SMA map in which the CO emission region is barely resolved, a more definitive mass comparison should be based on a higher spatial resolution interferometric image (as is possible using longer baselines with the SMA).

With post–main-sequence evolutionary tracks from Schaller et al. (1992) or Girardi et al. (2000), agreement between kinematic and evolutionary mass can be obtained if BP Psc is a giant star of mass about 1.8 $M_\odot$ at a distance from Earth of about 300 pc. If so, then the main-sequence progenitor would likely have been of late A or early F type, if BP Psc is a single star. The progenitor might have been of somewhat later spectral type if BP Psc is a spectroscopic binary (§ 4.5), or if it has already accreted a companion star (§ 4.10.2).

4.5. *Is BP Psc a Spectroscopic Binary Star?*

The radial velocities listed in Table 5 are based on cross-correlation with radial velocity standards. For the three 2006 epoch spectra, we used the atmospheric B band (6860–6890 Å) to ensure proper wavelength corrections and to correct time variations of the zero-point wavelength shift due to changing observing conditions (temperature and pressure) over many nights. Thus, the radial velocity errors given in Table 5 for these 2006 epoch spectra include all uncertainties of which we are aware. In the 1996 epoch spectra of BP Psc, telluric lines near 5921 Å could be identified, but not in the 1996 epoch radial velocity standards for which any telluric lines were lost in a forest of many photospheric lines. Therefore, using the above telluric lines from the two epochs, the two 1996 epoch BP Psc spectra were shifted into the 2006 September 1 spectrum's rest frame. They were then cross-correlated with the September 1 spectrum to obtain radial velocities. All errors are included in the 1996 epoch radial velocity measurements listed in Table 5, including the September 1 velocity error added in quadrature with cross-correlation errors. Relative

to the radial velocity on September 1, the velocity on 1996 July 12 was more positive by 0.78 ± 1.52 km s^{-1}, while the 1996 October 10 velocity was more positive by 4.06 ± 2.00 km s^{-1}.

Variable Stars One-shot Project (VSOP; Dall et al. 2007) observed BP Psc on 2006 June 30 (UT) and July 14 (UT), and high-precision radial velocities[20] from these data are -12.9 and -13.5 km s^{-1} with a conservative 1 σ uncertainty of 10 m s^{-1}. In addition, Torres et al. (2006) observed BP Psc 11 times and their measured mean radial velocity is -5.8 ± 2.0 km s^{-1}. They flagged BP Psc as SB1 and classified it as G9 IIIe. Dall et al. (2007) also note a hint of a secondary in their cross-correlation function (T. Dall 2007, private communication). Therefore, BP Psc may be a binary star.

The range of radial velocities reported by Torres et al. (2006), Dall et al. (2007), and in Table 5 covers $\sim$10 km s^{-1}. If we assume that the mass of BP Psc is 1.5 $M_{\odot}$ and if it is orbited by a 0.1 $M_{\odot}$ companion at a distance of 10^{12} cm, then BP Psc's projected orbital velocity would be $\sim$10 km s^{-1}. Thus, such a possibility is consistent with currently available radial velocity data. If BP Psc is a pre–main-sequence star, the existence of an unseen M-type secondary of 0.1 $M_{\odot}$ (or greater) would widen the discrepancy between the estimated kinematic and evolutionary masses (§ 4.4).

At this juncture, it seems prudent to retain the possibility that the modest secular variations in the measured radial velocities are due to scattering off dust particles in a revolving inhomogeneous envelope (in preference to orbital motion of a binary star). Based on the CO line profiles, $\sim$10 AU from the star (as per the dimensions of the scattered light AO image in Fig. 4), a characteristic dust orbital velocity is $\sim$10 km s^{-1}. Understanding the cause(s) of the velocity variations will require a comprehensive monitoring campaign.

4.6. *Dust Mass*

The SMA detected an 880 μm continuum flux density, S_{ν}, of 18 mJy (Table 3; Fig. 3). We assume that S_{ν} is generated entirely by dust particles in orbit around BP Psc and estimate the dust mass M_d in the usual way (e.g., Zuckerman 2001) from

$$M_d = S_{\nu} D^2 / k_{\nu} B_{\nu}(T_d). \quad (3)$$

Here D is the distance between Earth and BP Psc and k_{ν} is the dust opacity. At submillimeter wavelengths the Planck function B_{ν} can be written as $2kT/\lambda^2$. Following previous authors, we assume that $k_{\nu} = 1.7$ cm^2 g^{-1} at 880 μm, while recognizing that this value may be somewhat on the high side of the true value of k_{ν} (see the motivation for this choice of k_{ν} by Zuckerman & Becklin [1993], where the value 1.7 cm^2 g^{-1} at 800 μm wavelength was first introduced). This relatively large 880 μm dust opacity is carried by dust particles with radii of a few hundred microns according to the study by Pollack et al. (1994). The absence of a strong silicate feature in the 10 μm window (Fig. 5) is consistent with the presence of large particles.

As noted in § 4.3.2, BP Psc has little reddening (or bluing). Plausibly, optical light seen from BP Psc has pursued a complex path through the dusty envelope, undergoing both absorption and scattering. If, in addition, there is a wide range of particle sizes, from smaller to larger than the wavelengths of interest, then the dominant particles at visual wavelengths are apt to have sizes comparable to these wavelengths and changes in color should be minimal.

[20] Based on data provided by the VSOP collaboration, through the VSOP wiki database operated at ESO Chile and ESO Garching.

In part because there is no precedent for a giant star with an SED like that of BP Psc, we estimate dust masses by considering some results from debris disk studies of main-sequence stars. The SED of BP Psc indicates that orbiting dust is present over a wide range of temperatures. In addition to the hot dust at $\sim$1500 K and warm dust at 210 K, we can be quite confident that a substantial mass of cold dust grains is also present. Here we assume the model of a 10 Myr old, 5000 K star, $\sim$100 pc from Earth. In this case the semimajor axis of the molecular (CO) disk is 60 AU. Blackbody grains this far from BP Psc that are irradiated by the unattenuated stellar radiation field will be at 36 K, while 210 K blackbody grains will orbit only $\sim$2 AU from BP Psc. It is hard to conceive of a situation where all the dust would be located so much closer to the star than the molecular gas. Thus, in addition to the 1500 and 210 K dust particles, there should also be dust at temperatures too cold to have been detected by *IRAS*. We can estimate the relative amounts of warm and cold dust in the following way.

Williams and collaborators (Williams et al. 2004; Najita & Williams 2005; Williams & Andrews 2006) have measured the 850 μm flux density from eight stars (HD 8907, HD 14055, HD 15115, HD 21997, HD 107146, HD 127821, HD 206893, HD 218396) with *IRAS*-measured far-IR excess emission. We fitted blackbodies to the *IRAS* fluxes for these eight stars and compared the expected blackbody flux density at 850 μm to the Williams et al. measurement. In each case, the measured 850 μm flux density fell below the blackbody flux density, by factors ranging between 2.5 and 6, and, on average, by about a factor of 4. From Figure 6 we see that the 880 μm flux density of BP Psc lies within a factor of 2 of the plotted 210 K blackbody line. The most natural explanation of such an elevated 880 μm flux density is the presence of cold dust not seen by *IRAS*. An unambiguous example of this phenomenon is Hen 3-600 in the TW Hya association, where the 850 μm flux density lies well above the Rayleigh-Jeans blackbody extrapolation of the far-IR emission (Fig. 2 in Zuckerman 2001).

Based on the preceding discussion, for estimation of dust masses, we assume that 50% of the 880 μm flux density (i.e., 9 mJy) is generated by dust particles at 210 K and the other 9 mJy by cold dust at 36 K. Since some or even all of the eight Williams et al. stars likely are orbited by some cold dust responsible for some of the 850 μm emission, this 50/50 division of the 880 μm flux density is probably somewhat overly generous in favor of warm dust at BP Psc.

With $k_{\nu} = 1.7$ cm^2 g^{-1} and a flux density of 9 mJy at 880 μm, for a 10 Myr old star 100 pc from Earth, the mass of dust at 36 K is 4.3×10^{27} g, or 0.7 $M_{\oplus}$. For the 3 and 20 Myr old stars in Table 6, this mass would be roughly a factor of 2 larger and smaller, respectively. At each age, if the flux density carried by 210 K dust is also 9 mJy, then the mass of 210 K dust is about a factor of 6 smaller than the mass of 36 K dust.

If, instead, BP Psc is a giant star at 300 pc, then the implied disk radius would be $\sim$180 AU and dust masses would be an order of magnitude larger, or 7 $M_{\oplus}$. In addition, as mentioned above, $k_{\nu} = 1.7$ cm^2 g^{-1} may somewhat overestimate the dust opacity at 880 μm, in which case the dust mass would be even larger. For example, for the perhaps somewhat similar giant star HD 233517, Jura (2003) adopted an 880 μm opacity about 5 times smaller than 1.7 cm^2 g^{-1}. (See § 4.10 for additional discussion of HD 233517.)

4.7. *Gas Mass and Gas-to-Dust Ratio*

As noted in § 3, the upper limit to the ^{13}CO, $J = 2$–1 line intensity implies that the ^{12}CO opacity is <14 if the isotopic ratios are solar (1/89). The ^{12}CO optical depth can also be estimated by

comparing the peak brightness temperature of the $J = 2$–1 and 3–2 lines; the latter should be about twice as large when both lines are thin and the excitation temperatures and source sizes are the same for both transitions. Another potential diagnostic of CO optical depth is comparison of the peak brightness temperature of the CO lines with the temperature of the dust grains at a given distance from BP Psc; the latter temperature can be calculated assuming that the grains are sufficiently large to radiate like blackbodies and the grains see the unattenuated heating flux from BP Psc. If the CO lines are optically thick and if the gas is heated only by collisions with the dust (but Qi et al. [2006] argue for extra heating of the gas relative to the dust at a given distance from TW Hya), then the CO brightness temperature and dust temperature should be the same.

In § 4.6 we noted that the blackbody dust temperature 60 AU from BP Psc would be 36 K if these dust particles see the unattenuated heating flux from the star. Notwithstanding the large quantity of warm dust close to BP Psc, this assumption could be reasonable given that the disk is likely flared. Specifically, if the total mass of 36 K dust (0.7 $M_\oplus$) estimated in § 4.6 is carried by particles with radii $\sim$100 μm, and if all these grains are located out near 60 AU, then they will all see unattenuated starlight if their vertical extent above the disk plane subtends only a modest few AU. While we cannot rule out the possibility of some cold dust "hidden" in the disk midplane closer to BP Psc than 60 AU, the feeble 880 μm flux density guarantees that the BP Psc disk carries much less dust mass than disks around most well-known classical T Tauri stars. For example, the dust mass at the 8 Myr old TW Hya is $\sim$30 times greater than at BP Psc, and the dust mass of some Myr old classical T Tauri stars is greater by yet another order of magnitude. The virtue of measurements in the optically thin 880 μm continuum is that they reveal most of the mass in dust particles with radii less than about a centimeter. Somewhat similar arguments would apply if BP Psc is a giant star 300 pc from Earth. For example, Jura (2003) models HD 233517 as a flared disk.

The peak CO source brightness temperatures in the 2–1 and 3–2 lines are $\sim$23 K (last column of Table 3). Given uncertainties in the CO source sizes (especially for the 2–1 line) and concomitant brightness temperature uncertainties, it is not possible to draw any strong conclusions about CO optical depths from the various comparisons mentioned two paragraphs above other than to say that the ^{12}CO optical depths appear to be not much less than unity. Future interferometric observations of the CO lines with higher spatial resolution than those presented here might go a long way in clarifying the issue of optical depth. Detection of ^{13}CO would also be helpful, although this may not be easy given the long integration time (245 minutes) devoted to the ^{13}CO $J = 2$–1 line at the 30 m telescope.

We estimate a lower limit to the mass in H_2 molecules (in solar masses) using equations in Scoville et al. (1986). For CO, their expression reduces to

$$M_{H_2} = A \times 10^{-16}\ M_\odot (T_x + 0.92)\left(e^{B/T_x}\right) \times \left(\frac{\tau}{1 - e^{-\tau}}\right) \frac{S_{CO}(\text{Jy km s}^{-1}) D^2(\text{pc})}{X_{CO}}, \quad (4)$$

where the quantities A and B take the values 1.43 and 16.6, respectively, for the $J = 2$–1 line and 0.28 and 32.2 for the $J = 3$–2 line.

If BP Psc is a T Tauri star, to derive H_2 masses, we adopt excitation temperature $T_x = 36$ K, $D = 100$ pc, and $X(\text{CO}) = [\text{CO}]/H_2 = 10^{-4}$. Assuming optically thin lines, both the 2–1 and 3–2 integrated CO line intensities imply H_2 column densities $\sim 4 \times 10^{20}$ cm^{-2} and corresponding H_2 masses $\sim 10^{-5}\ M_\odot$ or about 4 $M_\oplus$. The masses could be an order of magnitude larger if the ^{12}CO $J = 2$–1 line has an optical depth $\sim$10 as permitted by the ^{13}CO $J = 2$–1 nondetection, and larger still if the CO is depleted relative to H_2 compared to the interstellar ratio X(CO) (that we have taken to be 10^{-4}). In any event, 4 $M_\oplus$ should represent a firm lower limit to the H_2 mass, excepting the (minor) caveat that X(CO) might be as large as 1/4000 (Lacy et al. 1994) rather than 1/10,000.

Comparison of H_2 mass with the cold dust mass of 0.7 $M_\oplus$ $\sim$60 AU from BP Psc (§ 4.6) yields a gas-to-dust ratio by mass in the range between 6 and about 100. Within a few AU of BP Psc, where the 210 K dust resides, the gas-to-dust ratio is unknown.

If BP Psc is a giant star 300 pc from Earth, then the lower limit to H_2 mass would be about 40 Earth masses. Because the dust and gas masses both scale as distance from Earth squared, to first order the gas-to-dust ratio by mass would be the same as indicated in the preceding paragraph. In the binary model sketched in § 4.5, one envisions a 0.1 $M_\odot$ star spiraling inward by $\sim 5 \times 10^{11}$ cm. For material contained in a concomitant excretion disk of radius 180 AU, conservation of angular momentum implies a disk mass of order that of Jupiter, in good agreement with the observations provided that the CO $J = 2$–1 line is somewhat optically thick.

4.8. *Mass Accretion Rate*

Mass accretion onto BP Psc is implied by the large quantity of hot dust, optical veiling, and strong, broad (full width at 10% of peak flux $\sim$500 km s^{-1}) Hα emission (Fig. 9). The mass accretion rate is $\sim 10^{-8}\ M_\odot$ yr^{-1} based on the Hα 10% width and the relationship for pre–main-sequence stars shown in Figure 3 of Natta et al. (2004). An independent accretion rate can be estimated with the prescription given in White & Hillenbrand (2004). As indicated in § 4.3.1, we estimate the ratio of excess continuum flux to photospheric flux to be $\sim$0.4 or less in the spectral region near 6500 Å. (This ratio is designated "r" by White & Hillenbrand 2004.) Then, for a 10 Myr old star of 5000 K, the mass accretion rate in solar masses per year is $\sim 10^{-8}$ and the accretion luminosity is $\sim$25% of the underlying stellar luminosity (White & Hillenbrand 2004; R. White 2007, private communication). This would be a very large accretion rate for a star as old as 10 Myr; with the possible exception of TW Hya, we know of no other as large. Mass-loss rates for stars ejecting bipolar jets, as per BP Psc, are typically estimated to be a few percent of the mass accretion rates (Hartigan et al. 1995; J. Muzerolle & R. White 2007, private communication).

Should BP Psc be a post–main-sequence giant star, and if the excreted disk mass is comparable to the mass of Jupiter (§ 4.7), then with an accretion rate of $10^{-8}\ M_\odot$ yr^{-1}, the disk might last only 10^5 yr (see also § 4.10.2).

4.9. *A Bipolar Herbig-Haro Outflow from BP Psc*

Figures 10–12 reveal an extensive chain of HH objects, the shock-excited emission nebulae that trace mass outflows from young stars. The bipolar outflow extends to the northeast (position angle $\sim$24°) and southwest of BP Psc, consistent with the orientation of the polar axis of the circumstellar disk seen in our Keck AO observations. As discussed in § 3, we deduce that the side of the disk nearest to Earth is to the southwest; thus, we conjecture that the northeastern jet is probably the redshifted side, while the southwest jet is blueshifted.

The overall appearance of the outflow is roughly symmetrical; on each side of the central star, a narrow linear filament stretches

several arcminutes away from the star, beyond which one or more bow shocks are visible. The filaments are clumped and knotty, like beads on a string, consistent with internal shocks due to turbulence or velocity variations within the outflow. Table 7 and Figure 11 give the positions of the various components of the HH outflow. But the symmetry breaks down on closer inspection, revealing extensive differences between the two sides in shape and brightness. The northern HH objects are brighter and more extensive than the southern ones and are visible to a greater distance from the star. The bright southern bow shock, knot S4, is $\sim$2.7′ from BP Psc, while the prominent northern shocks N3–N6 are $\sim$3.25′, 3.95′, 4.25′, and 6.50′ from the star. There are faint suggestions of additional nebulosity at greater distances from the star (knots S5, S6, and N7 in Table 7), but deeper integration is necessary to confirm these low signal-to-noise ratio (S/N) detections.

At an estimated distance of $\sim$100 pc, the observed jet extends at least 0.25 pc, or 0.5 pc if the faint outer HH objects are confirmed. Its total extent may well be greater than this, extending outside our current field of view, since many T Tauri stars are known to launch multiparsec-long outflows (McGroarty & Ray 2004 and references therein). Deep observations of the region around BP Psc with larger fields of view will be required to determine the true physical size of the outflow.

The two sides also differ in the relative intensities of the Hα and [S II] emission lines (Figs. 10 and 11): the southern filament S3 is much brighter in [S II] than Hα, while the northern filament N1 is comparably bright in both. The two knots immediately southwest of BP Psc, S1 and S2, are visible in [S II] emission only. With the exception of these knots and the southern filament, the Hα emission generally extends over larger angular scales than the [S II] emission. In particular, for all the bow shocks, the leading edges are visible in Hα, while the [S II] is confined to further back behind the shock. This is entirely consistent with the bow shock plus Mach disk emission features of other similar outflows such as HH 34 (Reipurth et al. 2002).

Once away from the star, the northeastern and southwestern sides of the jet are not separated by 180° because the outflow overall is curved, not straight (Fig. 11, *third panel*). Close to the star, the inner filaments appear well collimated, but at larger distances the HH objects appear increasingly deflected toward the northwest. The three outer, low-S/N HH objects, knots S6, S7, and N8 (outside the field of view of Fig. 11), continue this curving pattern, with position angles increasingly far from the initial jet axis (Table 7). While precession has been invoked to explain curvature in other HH jets, that mechanism generally produces symmetrically curved, S-shaped outflows, in contrast to the morphology observed here. Instead, the BP Psc flow appears to be part of the rarer class of "C-shaped" outflows such as HH 334 and HH 366 (Bally et al. 1996; Bally & Reipurth 2001). It has been suggested that such shapes arise because of deflection of jets due to proper motion between the star and the surrounding nebula (i.e., a crosswind; see Lebedev et al. 2004). The proper motion of BP Psc (§ 4.2) toward the southeast is in a direction consistent with this model. From Figure 11, one deduces that, in the plane of the sky, the jet velocity is $\sim$17 times the velocity of the star, if the jet material were to completely lose the proper motion of the star at the outset of the outflow. This gives an upper limit to the jet velocity of $\sim$390 km s^{-1} (at an assumed distance of 100 pc). Since, in the model, the loss of the component of motion toward the southeast is due to the crosswind, the actual jet velocity is certainly less than 390 km s^{-1} and can be derived from measurements of proper motions of the HH objects along the direction of the jet.

After the discovery of the jet, we reexamined the red plates from the Digitized Sky Survey[21] and discovered that several components of the BP Psc jet complex are visible in those data (Fig. 11, *bottom panel*). This presented an 18 yr temporal baseline to check for proper motion of the clumps. Knot S4 (which is the brightest portion of the nebula, and thus easiest to detect in the DSS) does appear to move between the two epochs. Its apparent shift of $\sim$5.1″ over 18 yr implies a proper motion of 0.28″ yr^{-1}, corresponding to 125 km s^{-1} at a distance of 100 pc or 375 km s^{-1} at 300 pc. We caution, however, that the proper motion is a very tentative measurement, given the uncertainty in the distance to BP Psc, the limited S/N on the clumps in the DSS image, and the possibility of systematic offsets between the DSS and Lick PFCam astrometric solutions.

High-velocity jets are of course known from many pre–main-sequence stars, but also from a modest number of evolved, high-luminosity, protoplanetary and planetary nebulae (e.g., Sahai 2002). One of the more striking examples of the evolved class is Hen 2-90 (Sahai 2002; Sahai et al. 2002; Kraus et al. 2005; Garcia-Segura et al. 2005), which has been analyzed in various ways in various papers involving some combination of general mass outflow, binarity, an accretion disk, magnetic fields, and rapid rotation. Hen 2-90 is of much earlier spectral type than BP Psc, and the observed linear extent of the Hen 2-90 outflow (even taking into account the uncertain distances to both objects) is much less than that at BP Psc.

Due to the visual obscuration near BP Psc, the launch region for its jets is better studied at radio wavelengths. Reipurth & Bally (2001) summarize interferometric observations of centimeter wavelength continuum emission at young stars with associated jets. Accordingly, we used the VLA (see § 2.1) in an imaging search for X- (3.5 cm) and L-band (20 cm) emission, in part to learn more about the launch region of the jets. An additional motivation for these observations was measurement of the parallax of BP Psc. Loinard et al. (2005) demonstrate that, for T Tauri stars accompanied by moderately strong radio sources as per T Tauri itself, the Very Long Baseline Array can be employed to measure stellar distances with exquisite precision. Unfortunately, we measured only upper limits to the BP Psc flux densities: $<$120 μJy beam^{-1} at X band and $<$1.7 mJy beam^{-1} at L band. Hence, parallax measurements will require optical images.

4.10. *Origin of BP Psc*

4.10.1. *T Tauri Star*

A characteristic of most known classical T Tauri stars is association with interstellar nebulosity. In such cases, where stars are only a few Myr old, we know the stellar birthplace. However, by $\sim$10 Myr, interstellar nebulosity has generally dissipated and usually other methods must be used to deduce the birthplace of rare, surviving, classical T Tauri stars and the more common, weak-lined, post–T Tauri stars. Thus, for example, TW Hya, an isolated 8 Myr old classical T Tauri star, likely had its origin in the Lower Centaurus Crux region (e.g., § 6 in Zuckerman & Song 2004).

In contrast, if BP Psc is a pre–main-sequence star, then its birthplace is unclear. Unlike TW Hya, which belongs to an association with dozens of known members, so far we have been unable to identify any stars in the vicinity of BP Psc with similar

[21] The Digitized Sky Surveys were produced at the Space Telescope Science Institute under US Government grant NAG W-2166. The images of these surveys are based on photographic data obtained using the Oschin Schmidt Telescope on Palomar Mountain and the UK Schmidt Telescope.

Galactic space motions and ages $\leq$10 Myr. The center of the nearest known prominent interstellar cloud MBM 55 (e.g., Hearty et al. 1999) is $\sim$20° north of BP Psc, and MBM 55 is devoid of any evidence of recent star formation (L. Magnani 2007, private communication). In addition, tracing the proper motion of BP Psc back for 10 Myr brings it no closer to MBM 55 than it is now (with the caveat that the proper motion of MBM 55 is unknown due to lack of associated stars).

4.10.2. *Post–Main-Sequence Star*

If BP Psc is a post–main-sequence star, then one plausible model is that BP Psc was once a close binary star, perhaps of the W UMa class, and the secondary was consumed by the primary after the primary left the main sequence. Alternatively, the secondary might still be present (§ 4.5) and responsible for ejection of material from a common envelope formed with BP Psc. Rucinski (2006) estimates that W UMa stars comprise perhaps 1 in 500 of main-sequence FGK stars. The lifetime of a 1.8 $M_{\odot}$ star while a first-ascent red giant is a few times 10^8 yr (Iben 1991). If the disk mass is $\sim$0.001 $M_{\odot}$ (§ 4.7), at the current accretion rate of 10^{-8} $M_{\odot}$ yr^{-1}, the gaseous disk might last only 10^5 yr. Then we might expect to see the BP Psc phenomenon in about one first-ascent giant star in one million.

In a search of more than 40,000 luminosity class III giants, Zuckerman et al. (1995b) found none anywhere near as infrared bright as BP Psc. C. Melis et al. (2008, in preparation) searched $\sim$100,000 giant stars in the Tycho catalog for excess infrared emission and found BP Psc (if it is a giant) and another star of spectral type F, with some (but not all) characteristics similar to those of BP Psc, that may also be a first-ascent giant star. Earlier, Jura (2003) modeled the dusty first-ascent red giant HD 233517 as arising from engulfment of a low-mass companion star. However, at HD 233517, there is no direct evidence of a gaseous disk, hot dust, mass accretion, or mass outflow. Also, the dust around HD 233517 is rich in carbon-rich polycyclic aromatic hydrocarbon components (Jura et al. 2006), for which there is no evidence in the 10 μm spectrum of BP Psc (Fig. 5). Finally, the CO images of BP Psc indicate a gaseous disk radius of $\sim$180 AU if the star is 300 pc from Earth, while the Jura model for HD 233517 suggests that the radius of its dusty disk may be $\leq$50 AU.

Soker (1998) presents arguments in support of the binary progenitor model (e.g., Morris 1987) for bipolar planetary nebulae. Soker's expectation is that a large fraction of the first-ascent giant branch descendants of low-mass ($M \lesssim 2\ M_{\odot}$) stars in close (separation $\lesssim$10 AU) binary systems will interact with their companions and experience a common-envelope phase that is accompanied by intense mass loss. Although this model does not directly predict that such a high mass-loss rate first-ascent giant phase would involve the formation of a disk and jets, such structures nevertheless might be expected, given the close analogy with binary interactions (and resultant axisymmetric mass loss) following the AGB (e.g., Nordhaus & Blackman 2006).

5. CONCLUSIONS

We have studied the optically variable star BP Psc with a variety of observational techniques spanning radio to optical wavelengths. This previously neglected star might be one of the nearest and oldest known classical T Tauri stars. However, more likely, it is the first known example of a first-ascent, post–main-sequence giant star with an associated orbiting massive molecular disk, rapid gas accretion, and outflowing bipolar jets and HH objects. The disk may be the aftermath of accretion of an erstwhile or extant low-mass companion of BP Psc, with material excreted from a common envelope as the companion is enveloped by BP Psc as the latter expands during the first-ascent giant phase. Whatever the disk origin, planets may now be forming in it, a Gyr or more after the formation of BP Psc itself.

Additional measurements are obviously desirable, including frequent monitoring of radial velocities to establish whether or not BP Psc is a close binary, X-ray flux and spectrum, extensive study of the bipolar jets, high-resolution aperture synthesis of CO emission, and high-resolution AO and/or *Hubble Space Telescope* imaging in the near-IR. Most important, a measurement of trigonometric parallax should clarify the evolutionary state of BP Psc. However, because of uncertainty associated with mass accretion luminosity and preferential viewing orientation nearly in the disk plane, even when we know how far BP Psc is from Earth, we will not know exactly how luminous the underlying star is.

We thank Emily Rice, Greg Wirth, and Ian McLean for helping to obtain the epoch 2006 NIRSPEC data and Ms. Rice for aid in their reduction. We acknowledge the efforts of Richard Webb in obtaining epoch 1996 data and thank Frank Fekel and Russel White for contributions. We are very grateful to Katia Biazzo and Antonio Frasca for important help in classifying BP Psc. We thank the referee for constructive comments, especially for a suggestion to consider gravity-dependent line ratios. This research was supported in part by NASA grants to UCLA. Portions of this work were performed under the auspices of the US Department of Energy by Lawrence Livermore National Laboratory under contract DE-AC52-07NA27344, and also supported in part by the National Science Foundation Science and Technology Center for Adaptive Optics, managed by the University of California at Santa Cruz under cooperative agreement AST 98-76783.

REFERENCES

Bally, J., Devine, D., & Alten, V. 1996, ApJ, 473, 921
Bally, J., & Reipurth, B. 2001, ApJ, 546, 299
Baraffe, I., Chabrier, G., Allard, F., & Hauschildt, P. 1998, A&A, 337, 403
Baraffe, I., et al. 2003, A&A, 402, 701
Beckwith, S., & Sargent, A. 1993, ApJ, 402, 280
Biazzo, K., Frasca, A., Catalano, S., & Marilli, E. 2007, Astron. Nachr., 328, 938
Briceno, C., et al. 2007, ApJ, 661, 1119
Burrows, C., et al. 1996, ApJ, 473, 437
Cieza, L., Kessler-Silacci, J., Jaffe, D., Harvey, P., & Evans, N. 2005, ApJ, 635, 422
Cohen, M., et al. 1999, AJ, 117, 1864
Dall, T., et al. 2007, A&A, 470, 1201
Davis, G., Naylor, D., Griffin, M., Clark, T., & Holland, W. 1997, Icarus, 130, 387
de la Reza, R., Torres, C., Quast, G., Castilho, B., & Vieira, G. 1989, ApJ, 343, L61
de Ruyter, S., et al. 2006, A&A, 448, 641
Downes, R., & Keyes, C. 1988, AJ, 96, 777
Fekel, F., Webb, R., White, R., & Zuckerman, B. 1996, ApJ, 462, L95
Frasca, A., et al. 2003, A&A, 405, 149
———. 2006, A&A, 454, 301
Garcia-Segura, G., Lopez, J., & Franco, J. 2005, ApJ, 618, 919
Girardi, L., Bressan, A., Bertelli, G., & Chiosi, C. 2000, A&AS, 141, 371
Gregorio-Hetem, J., Lepine, J., Quast, G., Torres, C., & de la Reza, R. 1992, AJ, 103, 549
Gunther, H., Liefke, C., Schmitt, J., Robrade, J., & Ness, J. 2006, A&A, 459, L29
Hartigan, P., Edwards, S., & Ghandour, L. 1995, ApJ, 452, 736
Hearty, T., et al. 1999, A&A, 341, 163

Iben, I. 1991, ApJS, 76, 55
Jura, M. 2003, ApJ, 582, 1032
Jura, M., et al. 2006, ApJ, 637, L45
Klemola, A., Hanson, R., & Jones, B. 1987, AJ, 94, 501
Kraus, M., Borges Fernandes, M., de Araujo, F., & Lamers, H. 2005, A&A, 441, 289
Lacy, J., Knacke, R., Geballe, T., & Tokinaga, A. 1994, ApJ, 428, L69
Lebedev, S., et al. 2004, ApJ, 616, 988
Loinard, L., et al. 2005, ApJ, 619, L179
Low, F., et al. 2005, ApJ, 631, 1170
Magnani, L., Caillault, J.-P., Buchalter, A., & Beichman, C. 1995, ApJS, 96, 159
McGroarty, F., & Ray, T. 2004, A&A, 420, 975
McLean, I., et al. 1998, Proc. SPIE, 3354, 566
———. 2000, Proc. SPIE, 4008, 1048
Morris, M. 1987, PASP, 99, 1115
Moultaka, J., Ilovaisky, S., Prugniel, P., & Soubiran, C. 2004, PASP, 116, 693
Najita, J., & Williams, J. 2005, ApJ, 635, 625
Natta, A., Testi, L., Muzerolle, J., Randich, S., Comerón, F., & Persi, P. 2004, A&A, 424, 603
Nordhaus, J., & Blackman, E. 2006, MNRAS, 370, 2004
Padin, S., et al. 1991, PASP, 103, 461
Palla, F., Randich, S., Flaccomio, E., & Pallavinici, R. 2005, ApJ, 626, L49
Pollack, J., et al. 1994, ApJ, 421, 615
Qi, C., et al 2006, ApJ, 636, L157
Reipurth, B., & Bally, J. 2001, ARA&A, 39, 403
Reipurth, B., Heathcote, S., Morse, J., Hartigan, P., & Bally, J. 2002, AJ, 123, 362
Rucinski, S. 2006, MNRAS, 368, 1319
Sahai, R. 2002, Rev. Mex. AA, 13, 133
Sahai, R., et al. 2002, ApJ, 573, L123
Sanchez-Blazquez, P., et al. 2006, MNRAS, 371, 703
Schaller, G., Schaerer, D., Meynet, G., & Maeder, A. 1992, A&AS, 96, 269
Scoville, N., Carlstrom, J., Padin, S., Sargent, A., Scott, S., & Woody, D. 1994, in IAU Colloq. 140, Astronomy with Millimeter and Submillimeter Wave Interferometry, ed. M. Ishiguro & J. Welch (ASP Conf. Ser. 59; San Francisco: ASP), 10
Scoville, N., et al. 1986, ApJ, 303, 416
Siess, L., Dufour, E., & Forestini, M. 2000, A&A, 358, 593
Soker, N. 1998, ApJ, 496, 833
Stempels, H., & Gahm, G. 2004, A&A, 421, 1159
Suarez, O., et al. 2006, A&A, 458, 173
Torres, C., et al. 2006, A&A, 460, 695
Vogt, S., et al. 1994, Proc. SPIE, 2198, 362
Wallace, L., Livingston, W., & Bernath, P. 1994, An Atlas of the Sunspot Spectrum from 470 to 1233 cm^{-1} and the Photospheric Spectrum from 460 to 630 cm^{-1}, NSO Tech. Rep. 1994
Webb, R., et al. 1999, ApJ, 512, L63
Weinberger, A. J., et al. 2002, ApJ, 566, 409
White, R., & Basri, G. 2003, ApJ, 582, 1109
White, R., & Hillenbrand, L. 2004, ApJ, 616, 998
Whitelock, P., et al. 1995, MNRAS, 276, 219
Williams, J., & Andrews, S. 2006, ApJ, 653, 1480
Williams, J., et al. 2004, ApJ, 604, 414
Wizinowich, P., et al. 2006, Proc. SPIE, 6272, 7
Wood, K., Kenyon, S., Whitney, B., & Turnbull, M. 1998, ApJ, 497, 404
Zuckerman, B. 2001, ARA&A, 39, 549
Zuckerman, B., & Becklin, E. 1993, ApJ, 414, 793
Zuckerman, B., Forveille, T., & Kastner, J. 1995a, Nature, 373, 494
Zuckerman, B., Kim, S. S., & Liu, T. 1995b, ApJ, 446, L79
Zuckerman, B., Koester, D., Reid, I. N., & Hunsch, M. 2003, ApJ, 596, 477
Zuckerman, B., & Song, I. 2004, ARA&A, 42, 685